T.R

EGE UNIVERSITY

Graduate School of Applied and Natural Science

DRAG FORCE CORRELATIONS AND EFFECT OF CHARGED PARTICLES ON DRAG FORCE FOR PARTICLE-LADEN FLOWS

MSc. THESIS

Gizem ÖZLER

Chemical Engineering Department

İZMİR

2022

T.R.

EGE UNIVERSITY

Graduate School of Applied and Natural Science

DRAG FORCE CORRELATIONS AND EFFECT OF CHARGED PARTICLES ON DRAG FORCE FOR PARTICLE-LADEN FLOWS

Gizem ÖZLER

Supervisor: Prof. Dr. Mustafa DEMİRCİOĞLU

Second Supervisor: PD Dr. habil Holger GROSSHANS

Chemical Engineering Department

Chemical Engineering Second Cycle Programme

Izmir

2022

EGE ÜNİVERSİTESİ FEN BİLİMLERİ ENSTİTÜSÜ

ETİK KURALLARA UYGUNLUK BEYANI

EÜ Lisansüstü Eğitim ve Öğretim Yönetmeliğinin ilgili hükümleri uyarınca Yüksek Lisans Tezi olarak sunduğum "Drag Force Correlations and Effect of Charged Particles on Drag Force for Particle-laden Flows (Parçacık Yüklü Akışlarda Sürükleme Kuvveti Bağıntıları ve Yüklü Parçacıkların Sürükleme Kuvvetine Etkisi)" başlıklı bu tezin kendi çalışmam olduğunu, sunduğum tüm sonuç, doküman, bilgi ve belgeleri bizzat ve bu tez çalışması kapsamında elde ettiğimi, bu tez çalışmasıyla elde edilmeyen bütün bilgi ve yorumlara atıf yaptığımı ve bunları kaynaklar listesinde usulüne uygun olarak verdiğimi, tez çalışması ve yazımı sırasında patent ve telif haklarını ihlal edici bir davranışımın olmadığını, bu tezin herhangi bir bölümünü bu üniversite veya diğer bir üniversitede başka bir tez çalışması içinde sunmadığımı, bu tezin planlanmasından yazımına kadar bütün safhalarda bilimsel etik kurallarına uygun olarak davrandığımı ve aksinin ortaya çıkması durumunda her türlü yasal sonucu kabul edeceğimi beyan ederim.

04 / 02 / 2022

Gizem Özler

ÖZET

PARÇACIK YÜKLÜ AKIŞLARDA SÜRÜKLEME KUVVETİ BAĞINTILARI VE YÜKLÜ PARÇACIKLARIN SÜRÜKLEME KUVVETİNE ETKİSİ

ÖZLER, Gizem

Yüksek Lisans Tezi, Kimya Mühendisliği Anabilim Dalı

Tez Danışmanı: Prof. Dr. Mustafa DEMİRCİOĞLU

İkinci Tez Danışmanı: PD Dr. habil Holger GROSSHANS

Ocak 2022, 58 sayfa

Hesaplamalı Akışkanlar Dinamiği (HAD) aracı olan pafiX (patlama korumasında parçacık akışı simülasyonu), parçacık yüklü akışların elektrostatik yüklenmesi olayını modellemeye odaklanır. İki fazlı akışların HAD simülasyonlarında, parçacık dinamiklerini tahmin etmek için doğru sürükleme kuvveti modellemesi esastır. Mevcut sürükleme kuvveti korelasyonları ancak belirli akış durumları için mevcut olduğundan, genel olarak geçerli bir formülasyon eksikliği vardır. Özellikle, bu korelasyonlar, daha önce elektrostatik kuvvetlere maruz kalan parçacık yüklü akışlar için değerlendirilmemiştir.

Bu tez, sürükleme kuvveti modellemesinin elektrik yüklü parçacıkların akışı üzerindeki etkisini bildirmektedir. Bu etkiyi inceleyebilmek amacıyla pafiX'e farklı sürükleme kuvveti korelasyonları uygulandı. Ardından, sürtünme Reynolds sayısı 180 olan parçacık yüklü kanal akışının Eulerian-Lagrange yaklaşımı kullanılarak yüksek çözünürlüklü Doğrudan Sayısal Simülasyonu (DNS) gerçekleştirildi.

Simülasyon sonuçları genel olarak duvara yakın bölgedeki parçacıklar üzerinde sürtünme korelasyonunun güçlü bir etkisi olduğunu, duvarlardan uzaktaki parçacıklar üzerinde ise etkisinin küçük olduğunu ortaya çıkardı. Turboforetik sürüklenme nedeniyle, parçacıkların kanal duvarlarına yakın bir yerde biriktiği

görüldü. Yüksüz parçacıklar için simülasyonlarda, sürükleme kuvveti korelasyonuna bağlı olarak duvara yakın bölgedeki parçacık derişim profilinde büyük sapmalar görüldü. Buradan, bir parçacığı çevreleyen akışın yakınındaki bir duvar veya diğer parçacıklar tarafından bozulmasının, sürükleme kuvveti için önemli bir etki olduğu sonucuna varılmıştır.

Elektrostatik kuvvetler tarafından yönlendirilen yüklü parçacıkların, yüklü olmayan parçacıklara göre, duvara daha da yakın bir yerde biriktiği görüldü. Yüksüz durumların aksine, parçacıklar yüksek bir yük taşıdığında (bu incelemede 1 femto Coulomb), yakındaki bir duvarın ve parçacıların sürükleme kuvveti üzerindeki etkilerinin oldukça düşük olduğu görüldü. Sonuç olarak, yüklü ya da yüksüz tüm parçacıkların sürüklenmesi üzerinde hem yakınlarındaki parçacıkların ve hem de duvarların etkisinin göz önüne alınması gerektiği ortaya konulmuştur.

Anahtar Kelimeler: Parçacık yüklü akış, DNS, Sürükleme Kuvveti, Triboelektrik Şarj

ABSTRACT

DRAG FORCE CORRELATIONS AND EFFECT OF CHARGED PARTICLES ON DRAG FORCE FOR PARTICLE-LADEN FLOWS

OZLER, Gizem

MSc. in Chemical Eng.

Supervisor: Prof. Dr. Mustafa DEMIRCIOGLU

Second Supervisor: PD Dr. habil Holger GROSSHANS

January 2022, 58 pages

The Computational Fluid Dynamics (CFD) tool pafiX (particle flow simulation in explosion protection) focuses on modeling the electrostatic charging of particle-laden flows. In CFD simulations of two-phase flows, accurate drag force modeling is essential for predicting particle dynamics. However, since all existing drag correlations were established for specific flow situations, a generally valid formulation is lacking. In particular, these correlations have not been evaluated for particle-laden flows subjected to electrostatic forces.

This thesis reports on the effect of drag force modeling on the flow of electrically charged particles. To this end, we implemented different drag correlations in pafiX. Then, we performed highly-resolved Direct Numerical Simulations (DNS) using a Eulerian-Lagrangian approach of a particle-laden channel flow of a friction Reynolds number of 180.

The simulations generally revealed a strong influence of the precise drag correlation on particles in the near-wall region and a minor effect on the particles far from the walls. Due to their turbophoretic drift, particles accumulate close to the channel walls. For uncharged particles, the simulations show large deviations of the particle concentration profile in the near-wall region depending on the drag force

correlation. Therefore, the disturbance of the flow surrounding a particle by a nearby wall or other particles is important for its drag.

Driven by electrostatic forces, charged particles accumulate even closer to the wall. Contrary to the uncharged cases, when the particles carry a high charge (in our case one femto-coulomb), we found minor effects of a nearby wall and nearby particles on the drag force. In conclusion, for the investigated conditions, we propose to account for the effect of nearby particles and walls on the drag of charged and uncharged particles.

Keywords: Particle-laden flow, DNS, Drag Force, Triboelectric Charging

PREFACE

With the project "Optimization of Wet Grinding Parameters" that I carried out to complete my undergraduate education under the supervision of Prof. Dr. Mustafa Demircioglu, my interest in computational fluid dynamics started and with the internship at Physikalisch-Technische Bundesanstalt where I had the opportunity to work on the CFD tool, pafiX developed by PD Dr. habil Holger Grosshans. The choice of the subject of the master thesis was in line with the development of the CFD tool. At the same time, the effect of drag force modeling for charged particles was investigated, which has not been studied before.

I hope you will enjoy reading the thesis.

Gizem OZLER

IZMIR

09/01/2022

TABLE OF CONTENTS

PAGE

LIST OF FIGURES

LIST OF TABLES

1 INTRODUCTION

1.1 Significance of the Project

Particle-laden flow is a class of two-phase flow that consists of a particulate phase and a carrier fluid phase. They are encountered in various industrial processes such as; pneumatic conveying of solids, energy conversion processes (Mallouppas and van Wachem, 2013), fluidized bed reactors (Tabaeikazerooni, 2019). During these processes, particle-particle and particle-wall collisions occur and particles acquire electrostatic charges through contact and electrical charge exchange. The electrification of the particles leads to the formation of deposits, dangerous sparks and dust explosions that might cause serious loss of life and property damage. On the other hand, it might be useful in some processes such as electrostatic precipitators and powder coating (Bissinger and Grosshans, 2020). Therefore, it is necessary to improve the understanding of this phenomenon in order to contribute to the prevention of potential hazards and the development of processes using the electrification of particles. For this purpose, many experimental studies have been carried out, but it is not possible to obtain a definite conclusion as their results are not compatible with each other. This inconsistency can be attributed to uncertainties in the experimental conditions such as flow pattern, initial and boundary conditions, and electrification mechanism (Grosshans and Papalexandris, 2017; Matsusaka et al., 2010). In recent years, the focus has shifted to developing numerical tools that can easily overcome these uncertainties.

In order to study the electrification of particles during pneumatic conveying, (Grosshans and Papalexandris, 2017) developed a computational fluid dynamic tool ‘pafiX’ which is specialized in the highly accurate prediction of the electrostatic charging of powder flows. The tool is based on the Eulerian-Lagrangian approach in which the Eulerian framework is used to solve the Navier- Stokes equations for the fluid phase and the Lagrangian framework is used for the computation of the acceleration of every single particle. Also, particles are considered as a point mass, which means that particles are smaller than the relevant length scale, and the flow around particles is not resolved from the no-slip boundary condition on the particle. Instead, fluid velocities are interpolated on the particle locations and the effect of

particles on fluid flow is considered by using source terms. As a major interaction force, drag is important for understanding the momentum exchange between phases and to obtain particle trajectories. However, the tool is not able to compute the drag force directly and particle-fluid interaction is only can be taken into account by suitable closure models. As a result, appropriate drag force models should be implemented to improve the accuracy of the simulation.

1.2 Aim of the Project

Currently, in the pafiX, the estimation of the drag force is based on the classical drag force correlation by Putnam, 1961 which is strictly valid for uniform flow. However, there are many effects (effect of other particles, the effect of a near-wall) that can cause nonuniformity in the flow and they needed to be considered to improve the drag force modeling and thus the simulation results. One of our goals throughout this work is to apply an accurate drag force correlation that can capture the mentioned physical effects to make simulations more practical. Our second objective is to evaluate the importance of drag force modeling on the flow of charged particles.

The thesis is structured as follows; in Section 2., a literature review of drag force correlations is given. In Section 3, we explained the modeling of particle-laden flow (modeling of fluid and particulate phase), numerical methods and the simulation setup. Finally, in Section 4, simulation results are given and the results are compared.

2 LITERATURE SURVEY

Interphase interactions take place in many chemical engineering processes involving more than one phase, and a good understanding and modeling of these interactions is essential in order to develop more practical simulation tools. Depending on the properties of a system investigated, the drag force might contribute greatly to the total force acting on a particle. Therefore, the precision of the drag force models has a direct impact on the accuracy of simulations (Lapple and Sepherd, 1940). In the following, the definition and direct computation of the drag force with the proposed drag force models are examined.

2.1 Drag Force

Drag force occurs as a result of direct contact between a fluid and an immersed body when the relative velocity between fluid and the object is not zero. Drag force can be classified into two types; skin friction drag (also called viscous drag), and pressure drag (also called form drag). Skin friction drag occurs as a result of viscous stresses on a body that are tangential to the surface of the object, and pressure drag occurs as a result of pressure gradient around the body and pressure stresses are perpendicular to the surface of the body. Integrating the pressure and viscous stresses over the surface of the body in the direction of flow gives the total drag force on a particle given by following equations (Chorin et al., 1990);

$$\mathrm{d}F_{\mathrm{D}} = -P\mathrm{d}A\cos(\theta) + \tau_{\mathrm{w}}\mathrm{d}A\sin(\theta)\,, \tag{2.1}$$

$$F_{\mathrm{D}} = \int \mathrm{d}F_{\mathrm{D}} = \int (-P\mathrm{d}A\cos(\theta) + \tau_{\mathrm{w}}\mathrm{d}A\sin(\theta))\,. \tag{2.2}$$

Here, pressure and shear forces acting on a differential area '$\mathrm{d}A$' are '$P\mathrm{d}A$' and '$\tau_{\mathrm{w}}\mathrm{d}A$' respectively, and '$\theta$' is the angle that the outer normal of '$\mathrm{d}A$' makes with the positive flow direction. However, it is not feasible to compute drag force from the pressure and viscous stress on an object experimentally. Instead, Particle-Resolved Direct numerical simulations can be used to compute the forces exerted by fluid directly from the boundary conditions on the particle. On the other hand, experimental works are based calculation of overall forces on immersed bodies.

2.2 Drag Force Correlations

The drag force exerted on a body by surrounding fluid depends on the density of fluid (ρ_f), the relative velocity between the particle and the fluid (u_{rel}) and the shape of the body. Accordingly, the drag force on an immersed body can be expressed as

$$F_D = C_D \frac{\rho_f}{2} {u_{rel}}^2 A \,. \tag{2.3}$$

where, C_D is the drag force coefficient, and A (m^2) is the projected area normal to flow. The drag force coefficient is used to capture the effect of more complex dependencies such as particle shape and flow conditions. For a spherical particle the cross-sectional area normal to flow, A, can be calculated based on the particle diameter (d_p) as

$$F_D = C_D \frac{\rho_f}{2} {u_{rel}}^2 \frac{\pi {d_p}^2}{4} . \tag{2.4}$$

From eqn. (2.4), it is clear that the drag coefficient is a function of the particle Reynolds number ($Re_p = \frac{u_{rel} d_p}{\nu}$) where ν (m^2/s) is the kinematic viscosity. Also, the acceleration due to drag force (f_D) is given by

$$f_D = -\frac{3\rho_f}{4\rho_p d_p} C_D |u_{rel}| u_{rel} \,. \tag{2.5}$$

The first analytical solution to the Navier-Stokes equation at very low Reynolds numbers ($Re_p \ll 1$) was given by Stokes (1851), which provides a theoretical framework to the dynamic forces experienced by a particle moving through an infinite fluid. When ($Re_p \ll 1$), flow is considered as creeping flow (also known as Stokes flow) and in this flow regime, inertial forces are so small compared to viscous forces. Stokes obtained analytical solution to the Navier-Stokes equations neglecting the non-linear inertia terms.

Based on Stokes' calculation, drag coefficient for a single spherical particle the corresponding drag force closure can be given as

$$C_{\mathrm{D}} = \frac{24}{Re_{\mathrm{p}}}. \tag{2.6}$$

When Reynolds number increases, inertial forces become more important and Stokes' drag correlation becomes invalid. Later, Oseen (1910), have found out that inertial effect is not negligible away from sphere, and considering inertia terms, an improved expression for drag force coefficient is provided which is given below:

$$C_{\mathrm{D}} = \frac{24\left(1 + \frac{3Re_{\mathrm{p}}}{16}\right)}{Re_{\mathrm{p}}} = \frac{24}{Re_{\mathrm{p}}} + 4.5\,. \tag{2.7}$$

There are also other attempts to reach an extended analytical solution (Goldstein, 1929; Proudman and Pearson, 1957; Liao, 2002). However, these works are limited with low Reynold numbers due to complexity of flow pattern for higher Reynolds numbers.

A great number of experimental works have been conducted in order to obtain the relation between Reynolds number and drag coefficient. Collecting extensive data from previous experimental works, Lapple and Sepherd (1940), developed Standard Drag Curve (SDC) which is shown in Figure 2.1. Also, some of the correlations have been offered to approximate the SDC curve are given in Table 2.1.

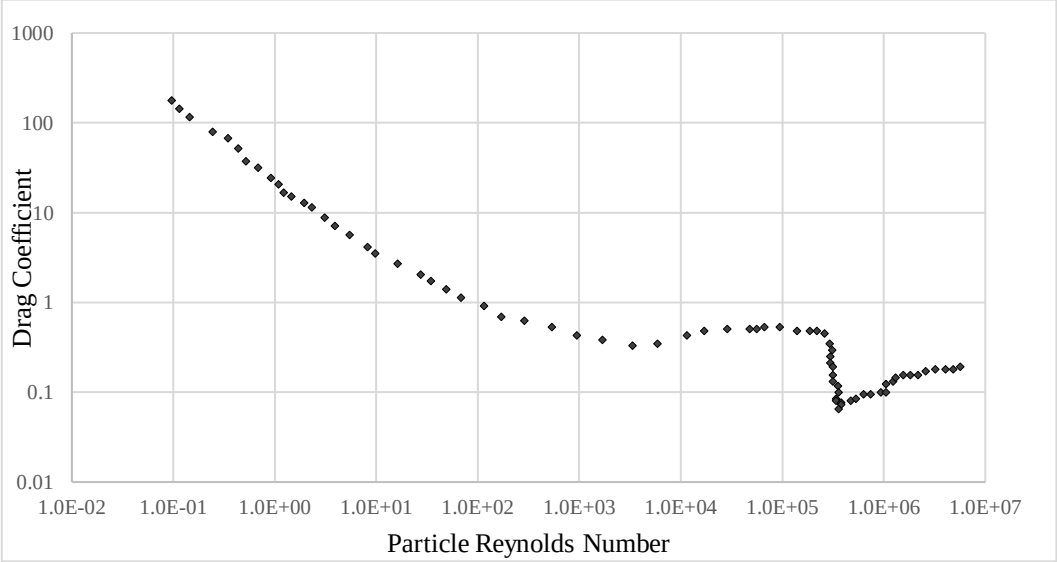

Figure 2.1. Standard Drag Curve for spherical particles (Lapple and Sepherd, 1940).

Readers who are interested in a comprehensive overview of empirical drag force correlations can visit Goossens' (2019) review. In the following sections drag force correlations for the non-isolated particles and in the presence of a nearby-wall are investigated.

Table 2.1. Correlations offered to approximate SDC curve

Correlation	$\boldsymbol{Re_p}$	**References**
$C_D = \frac{24}{Re_p}\left(1 + 0.15{Re_p}^{0.687}\right)$	$Re_p < 800$	(Schiller and Nauman, 1933)
$C_D = 0.48 + 28{Re_p}^{-0.85}$	$0.2 < Re_p < 2000$	(Gilbert et al., 1955)
$C_D = \frac{24}{Re_p}\left(1 + 0.15{Re_p}^{0.687}\right) + \frac{0.42}{\left(1 + 4.25 \times 10^4 {Re_p}^{-1.16}\right)}$	$Re_p < 3.10^5$	(Clift and Gauvin, 1970)
$C_D = 0.40 + \frac{4}{{Re_p}^{\frac{1}{2}}} + \frac{24}{Re_p}$	$Re_p < 3.10^5$	(Brauer and Mewes, 1972)

Finally, the drag force correlation by Putnam (1961), which is the correlation currently used in pafiX is given as,

$$C_{\mathrm{D}} = \begin{cases} \frac{4}{Re_{\mathrm{p}}}(6 + Re_{\mathrm{p}}^{2/3}) & Re_{\mathrm{p}} \leq 1000 \\ 0.424 & Re_{\mathrm{p}} > 1000 \end{cases}. \tag{2.8}$$

2.2.1 Drag Force Correlations Considering the Effect of a Near-Wall

The drag force correlations shown so far are only a function of the Reynolds number. However, flow pattern and wake structure for a particle close to a wall differs significantly. The effect of a nearby-wall is often to slow the motion of the particles and to change the transport properties of boundary layers (Zeng et al., 2009). The first asymptotic solution for the total hydrodynamic force on a spherical particle in rectilinear motion parallel to a wall was achieved by Faxén (1922). However, that solution is valid only for Stoke's flow regime and the distances greater than the radius of the particle. In that work, a drag factor, K_{wall}, is used for the effect of wall on drag force, which is defined as the ratio of drag in bounded fluid to the drag in unbounded fluid.

Goldman et al. (1967a), Goldman et al. (1967b) provided an analytical solution for the case in which the gap between the particle and the wall is so small compared to the radius of particle for wall-bounded flows. In order to consider the wall-slip and wall-shear interaction separately, two special cases are used; I) spherical particles moving parallel to a single plane wall in a quiescent fluid II) stationary particle in a shear flow and analytical solutions to these problems are solved and wall-modified drag coefficients offered by. Goldman's work showed that the effect of the wall is important if the gap between the particle and the wall is smaller than the particle diameter and can be neglected for distances of the order of ten particle diameters.

In order to consider the effect of a nearby-wall, we implemented the drag force correlation of Zeng et al. (2009) to pafiX.

- **Zeng et al. (2009)**

Using results from a large number of numerical simulations, Zeng et al. (2009), extended the particle Reynolds number range of Goldman's drag force correlations. They showed that the effect of the wall is still considerable for moderate Reynolds numbers and offered drag force closures for a particle translating parallel to the wall in a stagnant fluid and for a stationary particle in a wall-bounded linear shear flow. The composite drag law for a stationary particle in a wall-bounded linear shear flow is given by

$$C_{\mathrm{Ds}} = C_{\mathrm{Ds0}}\left(1 + \alpha_{\mathrm{s}} Re_{\mathrm{p}}{}^{\beta_{\mathrm{s}}}\right), \tag{2.9}$$

where;

$$\alpha_{\mathrm{s}} = 0.15 - 0.046(1 - 0.16\delta^2)\exp(-0.7\delta), \tag{2.10}$$

$$\beta_{\mathrm{s}} = 0.687 + 0.066(1 - 0.76\delta^2)\exp(-\delta^{0.9}), \tag{2.11}$$

$$C_{\mathrm{Ds0}} = \frac{24}{Re_{\mathrm{p}}}\left(1 + 0.138\exp(-2\delta) + \frac{9}{16(1+2\delta)}\right), \tag{2.12}$$

and δ, ($\delta = \frac{L}{d_{\mathrm{p}}} - 0.5$) is the normalized gap between the particle and wall.

The equation of the corresponding drag law for a particle moving parallel to a wall in a quiescent ambient flow is given by

$$C_{\mathrm{Dt}} = C_{\mathrm{Dt0}}\left(1 + \alpha_{\mathrm{t}} Re_{\mathrm{p}}{}^{\beta_{\mathrm{t}}}\right), \tag{2.13}$$

where;

$$\alpha_{\mathrm{t}} = 0.15\left[1 - \exp\left(-\sqrt{\delta}\right)\right], \tag{2.14}$$

$$\beta_{\mathrm{t}} = 0.687 + 0.313\exp\left(-2\sqrt{\delta}\right), \tag{2.15}$$

$$C_{\mathrm{Dt0}} = \frac{24}{Re_{\mathrm{p}}}\left[1.028 + \frac{0.07}{1+4\delta^2} - \frac{8}{15}\ln\left(\frac{270\delta}{135+256\delta}\right)\right]. \qquad (2.16)$$

The correlations are valid in the case $\delta \to 0$ and approach Schiller and Nauman's (1933) correlation in the limit $\delta \to \infty$.

2.2.2 Drag Force Correlations for Non-isolated Particles

By far we have given the drag force correlations which are only a function of the Reynolds number. However, it has been known from the previous works that, the presence of other particles alters the behavior of the fluid flow so the drag force on particles also changes significantly (Ergun and Orning, 1949; Wen and Yu, 1966). In order to develop a better drag force estimation, the effects of surrounding particles (crowding effect, swarming effect) are also needed to be taken into account. Many experimental and simulation studies have been performed to offer drag force correlations considering these effects. However, their definitions of Reynolds number and drag force correlations differ. In order to avoid confusion, both drag force and Reynolds number should be clearly defined before the correlations are presented.

In a system consisting of a steady-state fluid flow and a particulate phase, the fluid exerts two forces on the particle; drag force, $\boldsymbol{F}_{\mathrm{D}}$, (due to solid-fluid friction) and buoyancy force, $\boldsymbol{F}_{\mathrm{B}}$, (due to static pressure gradient). The sum of these two forces gives the total force on the particle, $\boldsymbol{F}_{\mathrm{f\to s}}$. Pressure gradient, $\boldsymbol{\nabla}P$, can be related with the drag and buoyancy forces as follows (Hoef et al., 2005),

$$-\boldsymbol{\nabla}P = \frac{N_{\mathrm{p}}}{V_{\mathrm{sys}}}\boldsymbol{F}_{\mathrm{f\to s}} = \frac{N_{\mathrm{p}}}{V_{\mathrm{sys}}}(\boldsymbol{F}_{\mathrm{D}} + \boldsymbol{F}_{\mathrm{B}}) = \frac{N_{\mathrm{p}}}{V_{\mathrm{sys}}}(\boldsymbol{F}_{\mathrm{D}} - V_{\mathrm{P}}\boldsymbol{\nabla}P), \qquad (2.17)$$

$$\boldsymbol{F}_{\mathrm{f\to s}} = \frac{1}{(1-\emptyset)}\boldsymbol{F}_{\mathrm{D}}. \qquad (2.18)$$

Where, N_{p} is the total number of particles in the system, V_{sys} is the volume of the system, V_{P} is the volume of a single particle and $\emptyset$, is the solid volume fraction ($\emptyset = \frac{N_{\mathrm{p}}V_{\mathrm{P}}}{V_{\mathrm{sys}}}$). In the literature, the total force ($\boldsymbol{F}_{\mathrm{f\to s}}$) which is the sum of buoyant and drag

force is also sometimes referred to as drag force. In this, we defined '$\boldsymbol{F}_{\mathrm{D}}$' as the drag force. Also, the drag force correlations given in this section are normalized by Stokes drag law;

$$|F_{\mathrm{D}}| = \frac{F_{\mathrm{D}}}{3\pi\mu d_{\mathrm{p}} U}. \tag{2.19}$$

where, U is the superficial velocity between the particle and the fluid and is defined as $U = \varepsilon|u_{\mathrm{s}} - u_{\mathrm{f}}|$, ε is the void fraction, u_{s} is the velocity of the particle, u_{f} is the velocity of the fluid, and Re_{p} is the Reynolds number defined as ($Re_{\mathrm{p}} = \frac{\rho_{\mathrm{f}} U d_{\mathrm{p}}}{\mu}$).

Drag force correlations for non-isolated case are mostly based on two different equations. The first one is the combinations of correlations of Kozeny (1927) and Carman (1956) given by

$$F_D\left(\emptyset, Re_{\mathrm{p}}\right) = F_D(\emptyset, 0) + f(\emptyset) Re_{\mathrm{p}}. \tag{2.20}$$

The first term in Kozeny and Carman's equation, $F_{\mathrm{D}}(\emptyset, 0)$, represents drag force in the limit of Stokes flow, and the second term accounts for the effects of inertia forces on drag.

The second type of drag force correlation are based on the closure of Dallavalle (1948), which is given in equation (2.21). In the equation, $F_{\mathrm{D}}\left(0, Re_{\mathrm{p}}\right)$ is for isolated particles and accounts for particle Reynolds number, and the 'β' accounts for the crowding effect.

$$F_D\left(\emptyset, Re_{\mathrm{p}}\right) = F_D\left(0, Re_{\mathrm{p}}\right)(1 - \emptyset)^{-\beta}. \tag{2.21}$$

There are also many experimental studies on the drag force correlations considering effect of the other particles. One of the earliest semi-empirical correlations is proposed by Ergun and Orning (1949), in which drag force is derived from pressure drop experiments in fixed beds with zero particle velocity. Ergun equation is based on Kozeny and Carman's equation which is valid only for dense

systems ($\emptyset \gg 0.20$) and for low and intermediate Reynolds numbers. The normalized form of Ergun's drag force is given by

$$F_D = \frac{150(1-\varepsilon)}{18\varepsilon^2} + 1.75\frac{Re_{\mathrm{p}}}{18\varepsilon^2}. \tag{2.22}$$

According to Ergun and Orning (1949), energy loss (pressure drop) is the sum of the kinetic energy loses due to inertial forces and viscous energy losses. The first and the second terms in the equation represent the viscous and Reynolds dependent inertial forces respectively.

Wen and Yu (1966), using settling experiments proposed a drag force correlation based on closure of Dallavalle (1948). Their correlation is valid for dilute systems and approaches Schiller and Nauman's (1933) drag force relation in the limit $\varepsilon \to 1$. Here, the drag coefficient, C_{d}, depends only on Reynolds number. Their correlation is applicable to high and low Reynolds number regimes:

$$F_D = \frac{Re_{\mathrm{p}}}{24} C_{\mathrm{D}} \varepsilon^{-3.65}, \tag{2.23}$$

$$C_{\mathrm{D}} = \begin{cases} \frac{24}{Re_{\mathrm{p}}}\left(1 + 0.15 Re_{\mathrm{p}}{}^{0.687}\right) & Re_{\mathrm{p}} \leq 1000 \\ 0.44 & Re_{\mathrm{p}} > 1000 \end{cases}. \tag{2.24}$$

(2.25)

A hybrid drag force correlation is proposed by Gidaspow (1994) to obtain a correlation valid for both dilute and dense flow systems, combining the correlations of Wen and Yu (1966) and Ergun and Orning (1949). Correlation of Gidaspow (1994) is given as;

$$F_{\mathrm{D}}(\varepsilon, Re_{\mathrm{p}}) = \begin{cases} \frac{150(1-\varepsilon)}{18\varepsilon^2} + \frac{1.75}{18\varepsilon^2} Re_{\mathrm{p}} & \varepsilon \leq 0.8 \\ \frac{C_{\mathrm{D}}}{24} Re_{\mathrm{p}} \varepsilon^{-3.65} & \varepsilon > 0.8 \end{cases}. \tag{2.26}$$

$$C_{\mathrm{D}} = \begin{cases} \frac{24}{Re_{\mathrm{p}}}(1 + 0.15 Re^{0.687}) & Re_{\mathrm{p}} \leq 1000 \\ 0.44 & Re_{\mathrm{p}} > 1000 \end{cases}. \tag{2.27}$$

Gidaspow's (1994) correlation covers the entire range of void fraction. However, there is a step change which causes a discontinuity on the curve and makes it unpractical to apply within that range. In order to ensure continuity between correlations, Gobin et al. (2003) proposed a new correlation given by

$$F_D = \begin{cases} F_{\mathrm{D(Wen\&Yu)}} & \emptyset \leq 0.3 \\ \min\left(F_{D(\mathrm{Wen\&Yu})}, F_{D(\mathrm{Ergun\&Orning})}\right) & \text{otherwise} \end{cases} . \tag{2.28}$$

Di Felice (1994), examined how the drag force deviates from the drag force in the presence of other particles by performing an experiment in which fluid flow through a packed fluidized bed with homogenous particle distributions assumption. The correlation is based on Dalavelle (1948)'s closure, in which β is also based on Reynolds number:

$$F_D = \frac{Re_{\mathrm{p}}}{24} C_{\mathrm{D}} \varepsilon^{-\beta} , \tag{2.29}$$

$$\beta = 3.7 - 0.65\exp\left(-\frac{\left(1.5 - \log\left(Re_{\mathrm{p}}\right)\right)^2}{2}\right). \tag{2.30}$$

Recently, with the increase in the computational power of the computers, it became more common to use computational simulations such as Lattice Boltzmann Simulation (LBM) and Immersed Boundary Method (IBM). These simulation methods are directly able to solve fluid flow around an object and provide accurate drag force closures. Lattice-Boltzmann simulations are first used by Hill et al. (2001a) for monodisperse static particle packings of simple cubic, face-centered cubic, and random arrays of spheres. Their correlation covers a solid volume fraction range of $0.001 \leq \emptyset \leq 0.6$ for low Reynolds numbers. They later extended their work to moderate Reynolds numbers, up to $Re_{\mathrm{p}} \leq 100$ (Hill et al., 2001b). However, their functions are not continuous and their closure is valid for lower Reynolds numbers. Benyahia et al. (2006) covering a full range of Reynolds number and fluid volume fraction, modified the correlation of Hill et al. (2001) and offered a continuous correlation. van der Hoef et al. (2005) offer a correlation using LBM for both mono- and bi-disperse sphere packings and for low Reynolds numbers (Re_{p}<<1).

Beetstra (2007), extended their work to higher Reynolds numbers (Re_{p}<<1000) for monodispersed particles and they offered the following closure:

$$F_D(\emptyset, Re_{\mathrm{p}}) = \frac{10\emptyset}{(1-\emptyset)^2} + (1-\emptyset)^2\left(1 + 1.5\emptyset^{\frac{1}{2}}\right) + \frac{0.413 Re_{\mathrm{p}}}{24(1-\emptyset)^2}\left[\frac{(1-\emptyset)^{-1} + 3\emptyset(1-\emptyset) + 8.4 Re_{\mathrm{p}}{}^{-0.343}}{1 + 10^{3\emptyset} Re_{\mathrm{p}}{}^{\frac{-(1+4\emptyset)}{2}}}\right]. \quad (2.31)$$

In the following paragraphs, the correlations that we have applied to pafiX in sub-sections are given. In the selection of correlations, their applicability to a very dilute case and low Reynolds number range are considered.

- **Tang et al. (2014):**

Tang et al. (2014), using Immersed Boundary Method, performed simulations for flow past fixed assemblies of monodisperse spheres in a face-centered-cubic array and for random distributions. Their correlations based on the closures of Kozeny (1927), Carman (1956) and covers a wide range of solids volume fractions ($0.0 \leq \emptyset \leq 0.6$) and particle Reynolds number ($50 \leq Re_{\mathrm{p}} \leq 1000$). The correlation by Tang et al. (2014) is given by

$$F_D(\emptyset, Re_{\mathrm{p}}) = \frac{10\emptyset}{(1-\emptyset)^2} + (1-\emptyset)^2\left(1 + 1.5\emptyset^{\frac{1}{2}}\right) + \left[0.11\emptyset(1+\emptyset) - \frac{0.00456}{(1-\emptyset)^4} + \left(0.169(1-\emptyset) + \frac{0.0644}{(1-\emptyset)^4}\right) Re_{\mathrm{p}}{}^{-0.343}\right] Re_{\mathrm{p}}. \quad (2.32)$$

- **Kravets et al., (2019)**

Kravets et al. (2019), using LBM simulations provided a drag force correlation for static random sphere packings. The correlation is applicable to a wide range of solid volume fraction ($0.0 \leq \emptyset \leq 0.4$) and Reynolds numbers ($Re_{\mathrm{p}} \ll 500$):

$$F_{\mathrm{D}}(\emptyset, Re_{\mathrm{p}}) = \frac{10\emptyset}{(1-\emptyset)^2} + (1-\emptyset)^2\left(1 + 1.15\emptyset^{\frac{1}{2}}\right) + \left[0.1695\emptyset(1+\emptyset) - \frac{0.004321}{(1-\emptyset)^4} + \left(0.0719(1-\emptyset) + \frac{0.02169}{(1-\emptyset)^4}\right) Re_{\mathrm{p}}{}^{-0.2017}\right] Re_{\mathrm{p}}. \quad (2.33)$$

In order to consider the crowding effect, drag force correlation of Tang et al. (2014) and Kravets et al. (2019) are applied to pafiX. However, these correlations are known to be applicable only for stagnant particles. Therefore, we also applied the correlation of Tang et al. (2016), which is based on moving particles, to compare the effect of particle mobility on drag force.

- **Tang et al. (2016)**

Tang et al. (2016), extended their previous work Tang et al. (2014) for dynamic suspensions of spherical particles. Drag force correlation they offered is given by

$$F_D(\emptyset, Re_{\mathrm{p}}, Re_{\mathrm{T}}) = \frac{10\emptyset}{(1-\emptyset)^2} + (1-\emptyset)^2\left(1 + 1.5\emptyset^{\frac{1}{2}}\right) + \left[0.11\emptyset(1+\emptyset) - \frac{0.00456}{(1-\emptyset)^4} + \left(0.169(1-\emptyset) + \frac{0.0644}{(1-\emptyset)^4}\right) Re_{\mathrm{p}}{}^{-0.343}\right] Re_{\mathrm{p}} + 2.98 Re_{\mathrm{T}} \frac{10\emptyset}{(1-\emptyset)^2}. \quad (2.34)$$

Here, the last term considers the effect of particle mobility on drag force. Re_{T} is the particle Reynolds number based on particle velocity fluctuations and can be related with the particle Reynolds number as

$$Re_{\mathrm{T}}\left(Re_{\mathrm{p}}, \frac{\rho_P}{\rho_f}\right) = 2.108 Re_{\mathrm{p}}{}^{0.85}\left(\frac{\rho_P}{\rho_f}\right)^{-0.5}. \quad (2.35)$$

3 CFD METHODOLOGY, MATHEMATICAL MODEL AND SIMULATION SETUP

3.1 CFD Methodology

The CFD tool pafiX is developed to achieve high accuracy simulation of electrically charged particle-laden turbulent flow. Overall methodology of CFD simulation is explained briefly in Figure 3.1 and in the following subsections.

3.1.1 Pre-Processing

Pre-processing starts with describing the fluid and the particulate phase with mathematical models given in Section 3.1. Geometry of the computational domain and mesh structure then should be selected (for the dimensions of the computational domain see Section 3.3). Defining the mesh structure, accuracy and resolution of simulations depend on number and arrangement of grids. Grid size should be small enough to minimize errors but as the number of grids increases, computational time also increases. Therefore, it is important to select an optimum grid size considering both the computational time and accuracy. A grid resolution study has been performed by Grosshans et al. (2021) and 256x144x144 number of grids are selected in x-,y- and z- directions which are uniform in x- and y- directions and stretched in z- direction. Grids are finer approaching the wall and coarser approaching the center of the channel in z- direction as many physical phenomena occur mostly in the near-wall region.

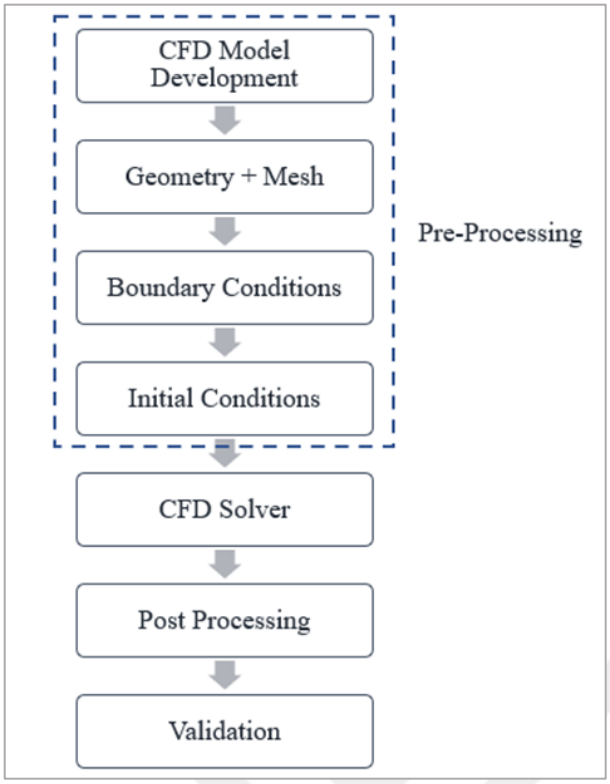

Figure 3.1. Flow Chart for CFD simulation.

Physical constraints of a system are defined by boundary conditions and are inputs to the simulation. Initial conditions are the specific type of boundary conditions that are only valid at the beginning. Initial conditions are highly important for stability and the rate of convergence of the simulations. For example, to decrease computing time, it is important to assign an initial condition which is very close to steady-state solution. Initial and boundary conditions of the simulation are given in Section 3.3. After assigning the conditions, simulations are run with the selected solver algorithm.

3.1.2 CFD Solver

The algorithm for the CFD solver is given in Appendix B. Numerical methods for the solution of the equations are given in this section. Criteria for convergence, stability are also discussed.

- **Numerical Solver**

For the fluid phase, second-order central difference scheme is used to compute convective, viscous, and pressure gradient terms. For the particulate phase time, derivative equations of the velocity of particles are solved using explicit first-order Euler forward integration, and particle positions are solved using second-order Crank-Nicolson integration. For the pressure-velocity correction, a modified version of the transient SIMPLE algorithm is used.

- **CFL number, relative tolerance**

In order to prevent instabilities on the computational domain, it is necessary to use Courant–Friedrichs–Lewy (CFL) number which is calculated as given below;

$$CFL = \frac{u\Delta t}{\Delta x}, \tag{3.1}$$

where, u is the velocity, Δt is time step size and Δx is the length interval. CFL number should be less than 1 in order to prevent a fluid parcel to go beyond one computational grid cell in one-time step. In our simulation, we adjusted a CFL number of 0.4 which is below 1.

Relative tolerance is the difference between current and previous solution divided by the current solution and it is used as convergence criteria. By reducing the relative tolerance, more accurate simulation results can be achieved, but this increases the computation time. In our simulation, relative tolerance is adjusted to 5.E-3.

3.1.3 Post-Processing and Validation

After the simulation is converged, the results can be analyzed. In this step, results for a property are averaged in time and space to eliminate fluctuations. Post-processing is a very important step to derive necessary conclusions, and depending on the presentation of data, simulation results might seem different. In our work, we used 140 number of bins in the wall-normal direction and bin size is getting smaller approaching the wall.

Finally, validation of the CFD solver can be achieved by comparing the data with previous DNS data in the literature.

3.2 Mathematical Model

In this section mathematical model that is employed in the simulation for gaseous and particulate phases are given. Mathematical model is based on conservation laws and represents the behavior of gaseous and the particulate phases.

3.2.1 Gaseous Phase

We simulated a turbulent particle-laden flow consists of a Newtonian carrier fluid with *N* particles using four-way coupled Eulerian-Lagrangian approach. The fluid phase is governed by Navier-Stokes equations and are solved in Eulerian framework in which the fluid flow properties are defined at a specific point in space-time. Fluid flow is assumed to be incompressible so that the equation for the fluid phase is given by the incompressible Navier-Stokes equation;

$$\boldsymbol{\nabla} \cdot \boldsymbol{u} = 0\,, \tag{3.2}$$

$$\frac{\partial \boldsymbol{u}}{\partial t} + (\boldsymbol{u} \cdot \boldsymbol{\nabla})\boldsymbol{u} = -\frac{1}{\rho_{\mathrm{f}}}\boldsymbol{\nabla} P + \nu \boldsymbol{\nabla}^2 \boldsymbol{u} + \boldsymbol{F}_{\mathrm{s}}\,. \tag{3.3}$$

Here, $\boldsymbol{u}$ is the fluid velocity vector, ρ_{f} is the density of the fluid, P is the fluid pressure and ν is the kinematic viscosity of the fluid.

For the purpose of achieving more realistic simulation results, four-way coupling approach (see Figure 3.2) is applied. Contrary to one way coupling, in four-way coupling, both the effect of the particle on the fluid and the interaction between the particles are taken into account. In this approach, these interactions are considered by implementing the source term, $\boldsymbol{F}_{\mathrm{s}}$, which accounts for the momentum transfer between the particle and the fluid.

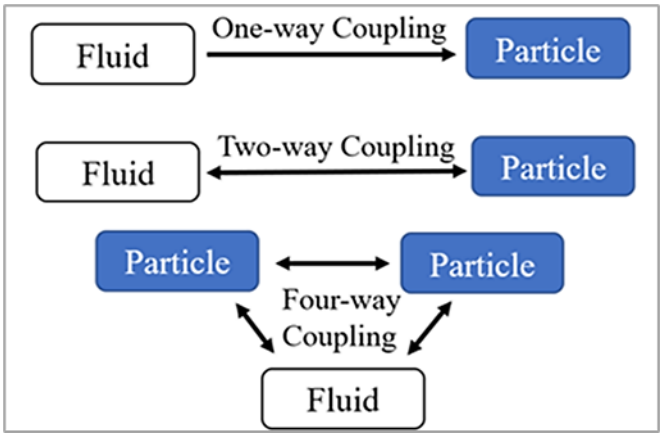

Figure 3.2. Couplings between particles and carrier fluid (Bi, 2015).

3.2.2 Particulate Phase

In our simulation, particles are rigid, perfectly spherical and their material density is the same. Point mass approach is employed so that particles are smaller than the grid cells and the effect of particles on fluid flow is taken into account by source term. Each particle is tracked individually in the Lagrangian framework and the acceleration of a single particle can be calculated based on the forces acting on them as follows;

$$\frac{\mathrm{d}\boldsymbol{u}_\mathrm{p}}{\mathrm{d}t} = \boldsymbol{f}_\mathrm{ad} + \boldsymbol{f}_\mathrm{el} + \boldsymbol{f}_\mathrm{coll} + \boldsymbol{f}_\mathrm{g}\,, \tag{3.4}$$

where, $\boldsymbol{u}_\mathrm{p}$ is the velocity of the particle, $\boldsymbol{f}_\mathrm{ad}$ is the aerodynamic drag acting on the particle, $\boldsymbol{f}_\mathrm{el}$ is the acceleration of the particle due to the electric field, $\boldsymbol{f}_\mathrm{coll}$ is the collisional acceleration, $\boldsymbol{f}_\mathrm{g}$ is the acceleration due to the net effect of gravity. Aerodynamic drag acceleration, $\boldsymbol{f}_\mathrm{ad}$ is given as (Crowe et al., 2012)

$$\boldsymbol{f}_\mathrm{ad} = -\frac{3\rho_\mathrm{f}}{8\rho_\mathrm{p} r_\mathrm{p}} C_\mathrm{D} |\boldsymbol{u}_\mathrm{rel}| \boldsymbol{u}_\mathrm{rel}\,, \tag{3.5}$$

where, C_D is the Putnam (1961)'s drag force correlation given by

$$C_{\mathrm{D}} = \begin{cases} \dfrac{4}{Re_{\mathrm{p}}}\left(6 + Re_{\mathrm{p}}^{2/3}\right) & Re_{\mathrm{p}} \leq 1000 \\ 0.424 & Re_{\mathrm{p}} > 1000 \end{cases}. \tag{3.6}$$

The acceleration due to electric field $\boldsymbol{f}_{\mathrm{el}}$, can be calculated as

$$\boldsymbol{f}_{\mathrm{el}} = \frac{Q\boldsymbol{E}}{m_{\mathrm{p}}}, \tag{3.7}$$

$$\boldsymbol{E} = -\boldsymbol{\nabla}\varphi, \tag{3.8}$$

where, Q is the charge of the particle, $\boldsymbol{E}$ is the electrical field strength, φ is the electrical potential, ρ_{el} is the electrical charge density and ε is the permittivity of fluid phase. It is assumed that electrical potential satisfies Poisson equation, ($\boldsymbol{\nabla}^2\varphi = \rho_{\mathrm{el}}/\varepsilon$), and so the permittivity of fluid is assumed to be the same as permittivity of vacuum. For a system with control volume of *V*, the sum of the charges of *N* number of particles is given as

$$\int \rho_{el}\mathrm{d}V = \sum_{i=1}^{N} Q_i \ . \tag{3.9}$$

3.3 Simulation Setup

A turbulent particle-laden flow in a channel between two parallel planar walls is simulated for electrically charged and uncharged particles. Our simulations are started without any particles for the fluid phase until we obtain a fully developed turbulent flow. After that, uniformly distributed particles are seeded inside the computational domain, as it is known that initial position of particles has not any effect on steady-state distribution of particles. Simulations have been run until the particles reach steady-state.

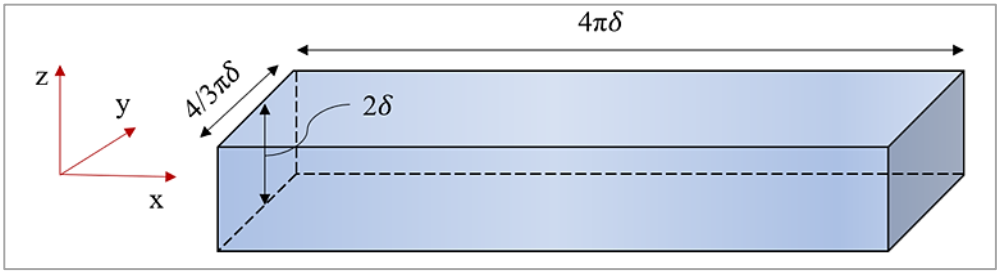

Figure 3.3 Representation of local computational domain.

In order to compare our simulation results with the work of Sardina et al., (2012), we adjusted initial conditions and dimensions according to the mentioned paper. In our computational domain, the x-, y- and z- axes points to the streamwise, spanwise and wall-normal directions, respectively (see Figure 3.3). Dimensions of the computational domain are ($4\pi\delta$, $4/3\pi\delta$, 2δ) where δ is the channel half-width. Periodic boundary conditions are applied on streamwise and spanwise directions means that when a property reaches the boundary of the computational domain, it is introduced from the opposite side again.

The fluid flow is driven by a constant pressure gradient. In order to compute the pressure gradient, friction Reynolds number ($Re_\tau = u_\tau \delta / v$) is used. Here, u_τ, ($u_\tau = \sqrt{\tau_w / \rho_f}$) is the friction velocity and τ_w is the shear stress at the wall. Based on friction Reynolds number (Re_τ = 180), constant external pressure gradient to impose the fluid flow is computed as -1.065 N/m^2 (see Appendix A).

By using the fixed density ratio in the reference paper, the material density of particles is calculated as 924 kg/m^3. For the wall-bounded turbulent flows Stokes number is given by

$$St^+ = \tau_p {u_\tau}^2 / \nu \,. \tag{3.10}$$

where, τ_p is the particle response time and calculated as

$$\tau_p = \frac{\rho_p d_p^2}{18 \rho_f \nu} \,. \tag{3.11}$$

In our simulation, all particles have the same size and based on the Stokes number in the reference paper ($St^+ = 1$), the diameter of particle is selected as 1.69×10^{-5}m. Inelastic collisions with the restitution coefficient of 0.9 is considered. Despite the collisions being considered as elastic collisions in the reference paper Sardina et al. (2012), it has been reported that it makes negligible differences in simulation results (Li et al., 2001).

Considering the electrical charges, we assumed that particles do not exchange charges through particle-particle and particle-wall collisions and so the particle charges are kept constant. Also, we assumed that there is no gravitational and lift force acting on the particle.

In order to reduce the computation time, simulations are performed in a parallel cluster, means that the computational domain has divided into smaller subdomains and are solved using set of computers simultaneously. For parallelization purposes, message passing interface (MPI) is used to exchange the data across boundaries of subdomains.

4 RESULTS AND DISCUSSION

In this section, results of the simulations for charged and uncharged cases are presented. Simulation results for different drag force correlations and for charged and uncharged cases have been discussed.

4.1 Uncharged Particles

In our work, evaluation of the simulations results is started from the uncharged case. In the following, we are going to investigate; how the concentration profile develops as time pass, what is the general pattern after particles reached the steady-state, what is the effect of post-processing methods on the results of simulations, and how does the drag force correlations affect the concentration profile for the uncharged case. Also, we compared our simulation results with the DNS study of Sardina et al. (2012) in order to validate our solver for the particulate phase. The solver for the gaseous phase has already been validated by Grosshans et al. (2021).

4.1.1 Temporal Evolution of Particle Concentration of Uncharged Case

As previously mentioned, we started the simulations from the fully developed turbulent flow and seeded uniformly distributed particles which have the same velocity as the fluid in that position. Uniform distribution of particles means that, at the beginning of the simulations, normalized particle concentration (particle concentration in a specific region divided by overall particle concentration) is equal to 1, every point in the computation domain.

Figure 4.1 shows normalized concentration profiles of the particles at the first 5% of the computational domain from the wall with respect to time using different drag force correlations. Particle concentration in the 5% of the channel is normalized by the overall particle concentration. It is a good property to check the convergence as many physical phenomena occur in the near-wall region. After particles have reached steady-state, the results of our simulations are sampled. By looking at the Figure 4.1, it is seen that our particles reached the steady-state and

any variable (velocity of fluid and particles, drag force, Reynolds number, etc.) can be averaged in space and time to eliminate fluctuations.

For all simulation cases, it is obvious that particles tend to accumulate in the near-wall region. At the beginning of the simulations, particle concentration in the near-wall region increases very fast due to the effect turbophoresis (will be discussed in the next section), however, accumulation rate decreases as the time past. The reason for this might be that the particle concentration decreases in the regions where the particles migrate, as the particles pass through the near wall region under the effect of turbophoresis. As the particle concentration decreases, accumulation rate of particles might also decrease.

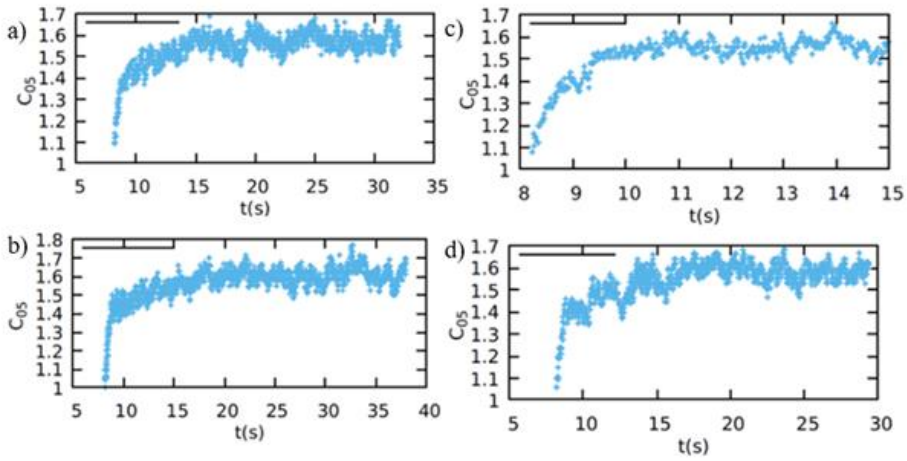

Figure 4.1. Temporal evolution of concentration profile in the 5% of the channel nearest to the wall using different drag force correlations. a) Putnam (1961) stat. part., b) Zeng et al. (2009) stat. part., c) Tang et al. (2014) stat. part d) Kravets et al. (2019) stat. part.

4.1.2 Results of Simulations for Uncharged Case

The particle Reynolds number with normalized distance from the wall is given in Figure 4.2. It should be mentioned that, for the cases in which drag force correlations for non-isolated particles are implemented, we used Particle Reynolds numbers based on superficial velocity, $Re_{\mathrm{p}} = \rho u_{\mathrm{rel}}(1-\emptyset)/\mu$. However, on the plot, we showed the Particle Reynolds number based on the relative velocity which does not depend on the fluid volume fraction, $Re_{\mathrm{p}} = \rho u_{\mathrm{rel}}/\mu$. Also, normalized distance, z^{+}, is the distance from the wall, normalized by viscous length, ($\delta_v =$

0.0001 m). Overall, it is seen that, for all simulation cases Re_p is lower than 0.1 means that we have Stoke's flow regime.

By looking at the Figure 4.2, we can see that different drag force correlations are giving slightly different particle Reynolds numbers. However, we have obtained the same trend in the particle Reynolds number profile for different cases. Firstly, particle Reynolds numbers very low in the near-wall region and it increases up to $z^+ = 7$. It continues to increase with fluctuations until $z^+ = 13$ and decrease through the center of the channel. As particle Reynolds number depends on absolute value of the relative velocity between fluid and particle u_{rel}, we also looked at the relative velocity profile given in Figure 4.3.

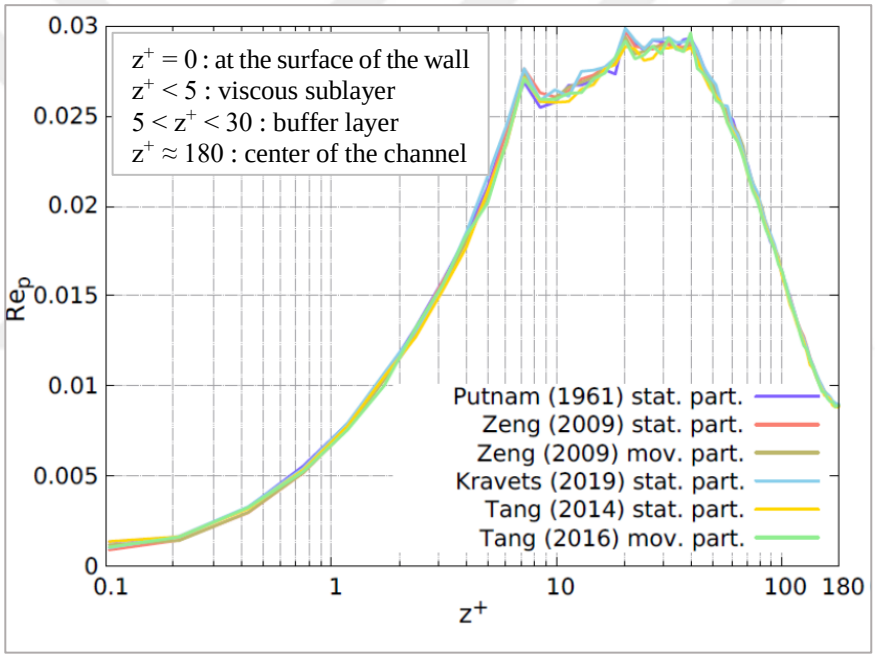

Figure 4.2. Particle Reynolds number with respect to normalized distance from the wall.

In Figure 4.3 relative velocity between the particle and the fluid in stream-wise direction with respect to normalized distance from the wall is given. It is seen that, due to lower fluid and particle velocities in the near-wall region, relative velocities are very small, it starts to increase moving away from the wall, and in the range of $1 \ll z^+ \ll 7$, the increase becomes greater. Through the center, relative velocity starts to decrease and particles lag behind the fluid for $z^+ \gg 20$. In the center, $z^+ = 180$, relative velocities are very small compared to viscous sublayer,

$3 < z^+ < 5$. Therefore, decrease in the particle Reynolds number $z^+ \gg 40$ is because of the decrease in relative velocity in that region.

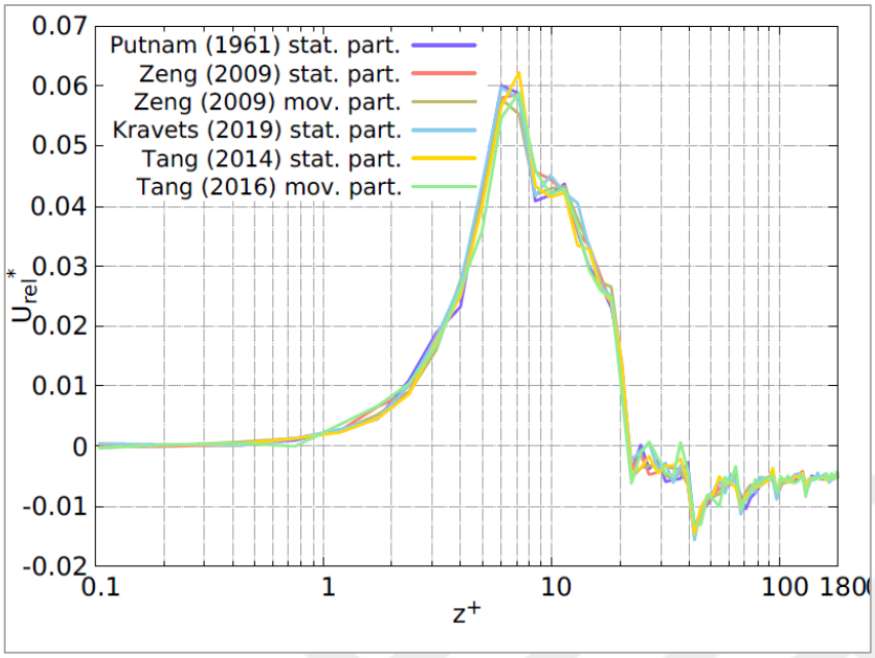

Figure 4.3. Normalized relative velocity with respect to normalized distance from the wall. (Here, relative velocity is normalized by the wall-friction velocity.)

In Figure 4.4 (for visualization purposes, Figure 4.5 shows the concentration profile only in the viscous sublayer), we compared concentration profiles using different drag force correlations and DNS data of Sardina et al. (2012). Before discussing the differences in results among different drag force correlations, we will look at the general pattern which is, the concentration of particles is higher in near-wall region. It has known that particles tend to accumulate in the near-wall region as a result of a phenomena called as 'turbophoresis', which is the tendency of particles to travel through lower turbulence energy levels. Therefore, as a result of difference in energy levels between local turbulence flow fields, preferential particle migration occurs, which leads in long-term accumulation in specific regions, mostly in viscous sublayer. On the other hand, a fraction of particles directly deposits in the near-wall region coming from higher turbulence levels and some of them moves to the wall by diffusion from the accumulation region (Marchioli and Soldati, 2002; Picciotto et al., 2005).

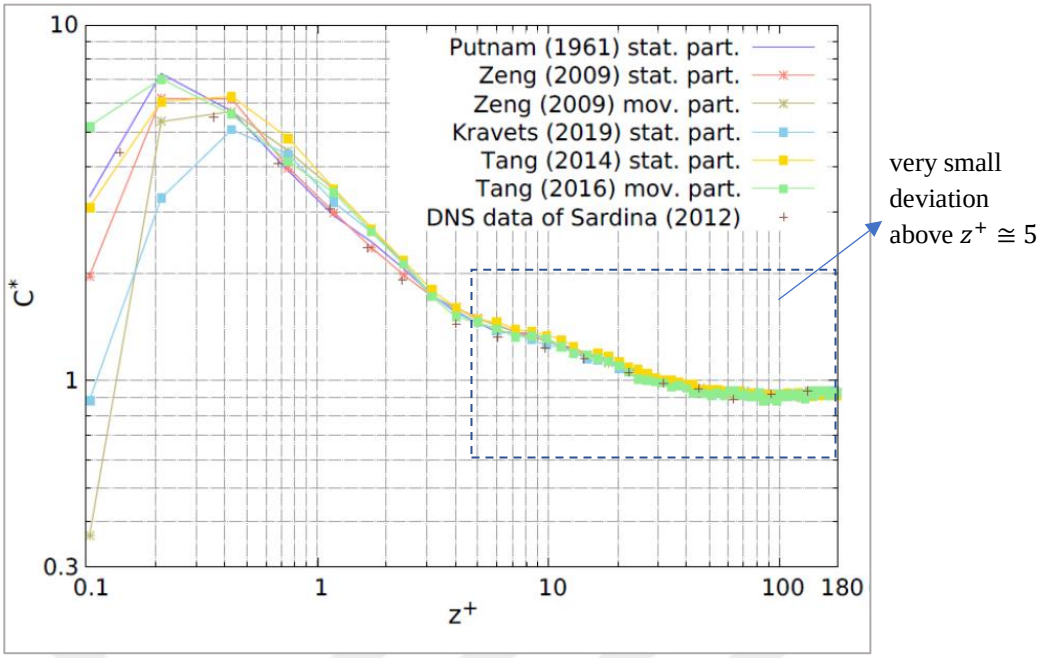

Figure 4.4 Comparison of concentration profiles using different drag force correlations and DNS data of Sardina et al. (2012) for uncharged case.

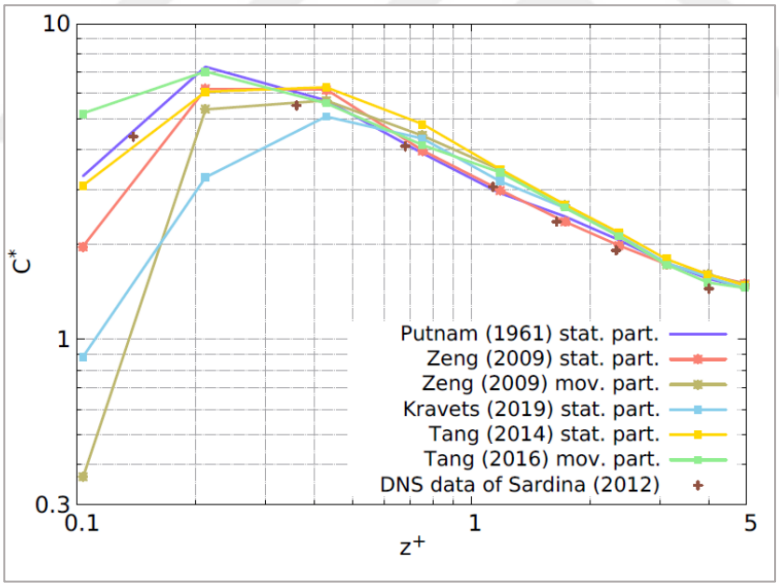

Figure 4.5 Figure 4.4 in the viscous sublayer.

This phenomenon also can be observed by looking at root mean square (rms) of fluid and particle velocity fluctuations in stream-wise and wall-normal direction given in Figure 4.6 and Figure 4.8 (for visualization purposes we focused on specific ranges which are given in Figure 4.7 and Figure 4.9). Rms of velocity fluctuation is the deviation from the average velocity (in time and space) and it is a

measure of intensity of the turbulence. The definition of rms velocity fluctuation is given below;

$$u_{\mathrm{rms}} = \left(\frac{1}{t_{\mathrm{end}}} \sum_{t=t_{\mathrm{initial}}}^{t_{\mathrm{end}}} |u_{\mathrm{i}}(t) - \bar{u}_{\mathrm{i}}|^2 \right)^{1/2}, \tag{4.1}$$

where, $\bar{u}_{\mathrm{i}}$ is the velocity averaged in time.

In channel flow there is a mean gradient of fluid and particle stream-wise velocity in the wall-normal direction. Due to the tendency of particles to be in lower energy turbulence regions, particles migrate through the near-wall regions, so that particle velocity fluctuations are higher than the fluid velocity fluctuations in the stream-wise direction. On the other hand, particles tendency to be in lower energy turbulence levels results with lower particle velocity fluctuations in the wall-normal direction.

It is also seen that the particle and fluid velocity fluctuations are different using different drag force correlations both in the stream-wise and wall-normal directions. Therefore, it is clear that, drag force modelling has a huge impact on particle dynamics as well as fluid dynamics.

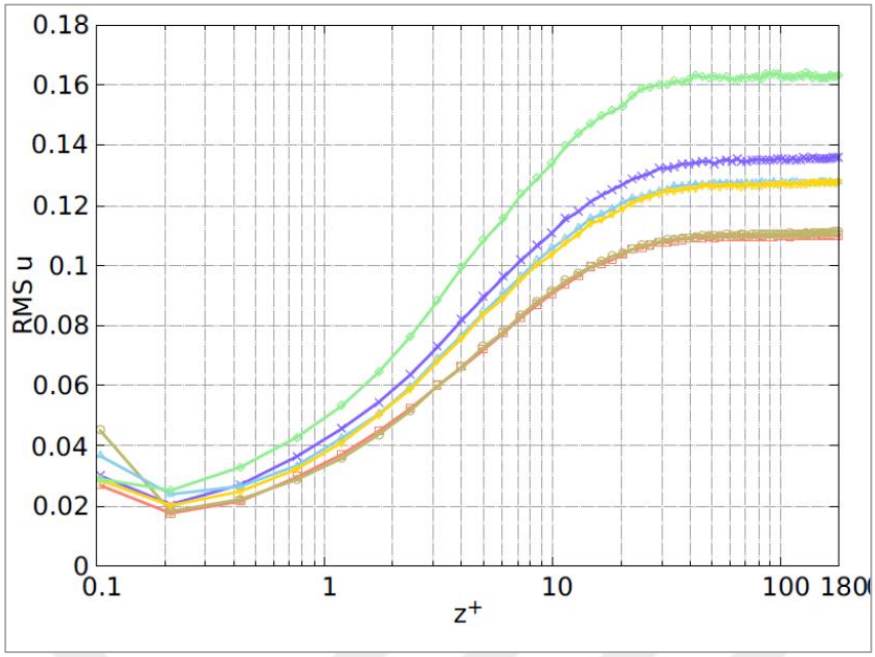

Figure 4.6. RMS of fluid and particle velocity fluctuations in stream-wise direction using different correlations.

Putnam (1961) is shown by (– , x); Zeng et al. (2009) for stationary particles is shown by (– , □); Zeng et al. (2009) for moving particles is shown by (– , O); Tang et al. (2014) is shown by (– , ∇); Tang et al. (2016) is shown by (– , ◊); Kravets et al. (2019) is shown by (– , Δ). In the figure, **lines** represent the fluid phase and **markers** represent the particle phase.

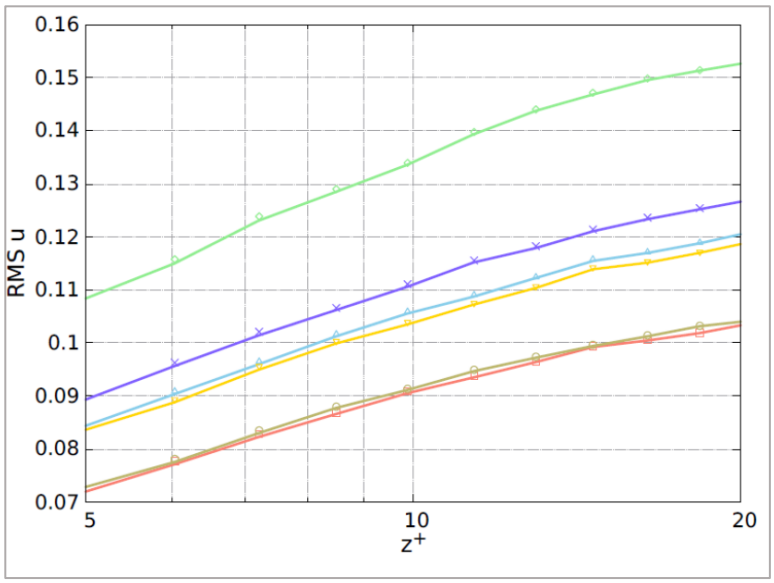

Figure 4.7. Figıre 4.6 in the range of $10 < z^+ < 20$.

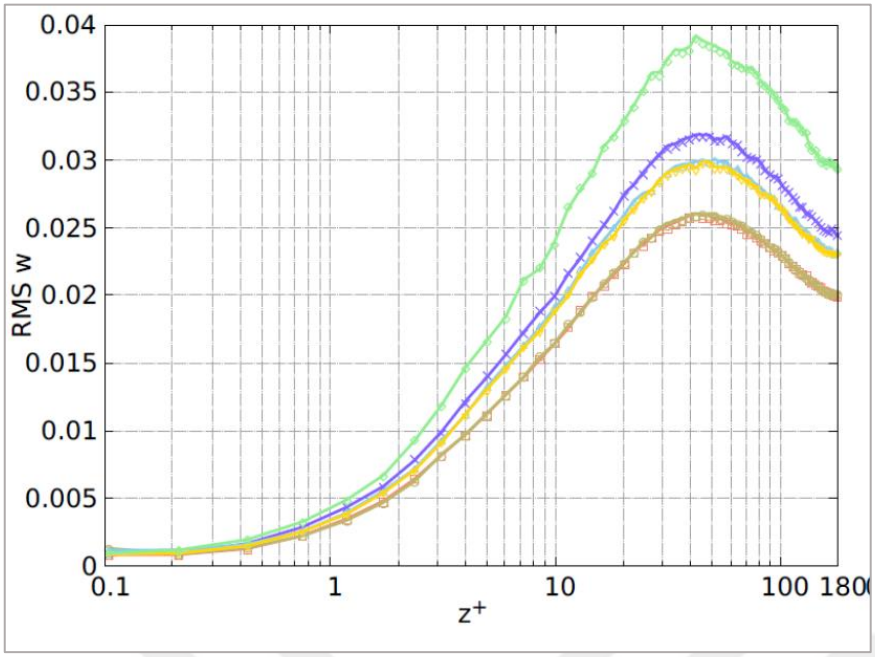

Figure **4.8**. RMS of fluid and particle velocity fluctuations in wall-normal direction using different correlations.

Putnam (1961) is shown by (– , x); Zeng et al. (2009) for stationary particles is shown by (– , □); Zeng et al. (2009) for moving particles is shown by (– , O); Tang et al. (2014) is shown by (– , ∇); Tang et al. (2016) is shown by (– , ◊); Kravets et al. (2019) is shown by (– , Δ). In the figure, **lines** represent the fluid phase and **markers** represent the particle phase.

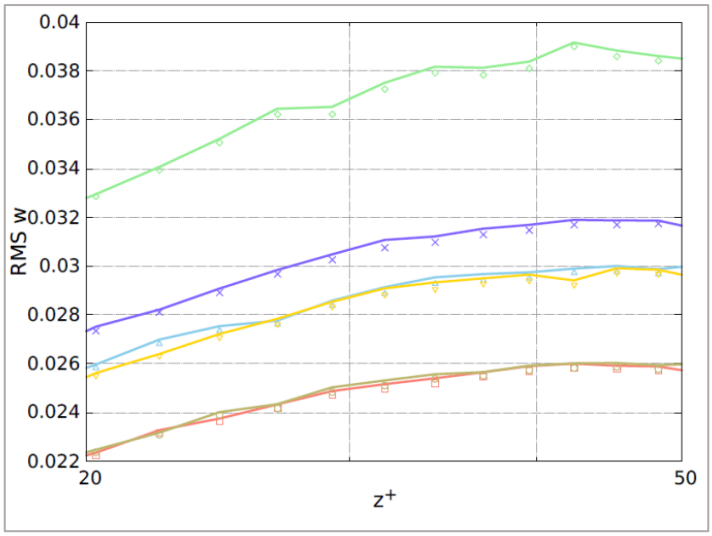

Figure 4.9. Figure 4.8 in the range of $10 < z^+ < 50$.

Comparing different correlations, deviations on the concentration profile are observed in the near-wall region (Figure 4.4 and Figure 4.5). Differences in the near-wall region using Putnam's correlation and using drag force correlations considering the effect of a nearby wall were expected, as they offered to be better able to predict physical phenomena in the near-wall region. Also, the effect of a nearby-wall has a clear trend which is to decrease the particle concentration in the near-wall region. Deviations using correlations for surrounding particles (deviations from the Putnam's (1961) case in the near-wall region using correlation of Tang et al. (2014), Tang et al. (2016) and Kravets et al. (2019) can be seen in Figure 4.4 and Figure 4.5) might be attributed to the higher particle concentration and non-uniformity of particle distribution in the near-wall region. However, we did not observe a clear trend for the effect of surrounding particles. We saw that, at moderate distances from the wall, the results obtained using different correlations are becoming the same. Therefore, we can conclude that, drag force modelling is important in the near-wall region, especially in the viscous sublayer and above $z^+ \cong 5$ might be insignificant.

Also, concentration profiles we obtained using Zeng et al.'s (2009) drag force correlations for two different cases (i. stationary particle in shear flow, ii. Moving particle in a quiescent flow) are different from each other. According to Zeng et al. (2009), the wall affects drag force on particles in two different ways. The first one is that, due to the additional shear that the wall creates, the total force acts on the particle is altered. The second one is, the presence of the wall breaks the symmetry around the particle due to local acceleration of fluid flow. Asymmetry around particle alters the pressure gradient around particle, which eventually affects the drag force. However, each case is known as they increase the drag force on the particle. Comparing Putnam's correlations results with the result using Zeng et al.'s (2009) correlation for a stationary particle in a linear shear flow, besides drag force modelling, this inconsistency can also be attributed to the fluid velocity profile, which is in our case a fully developed turbulent flow, and in Zeng et al. (2009)'s paper, a linear shear flow.

By looking at the results of correlations for non-isolated particles (Figure 4.4 and Figure 4.5) we have seen that, even we have a very dilute flow, there is still a

difference in concentration profiles using difference drag force correlations. Therefore, it might be necessary to implement a drag force correlation that consider the effects of other particles even at the dilute case. It should also be mentioned that, correlations that are considering non-isolated particles (Tang et al., 2014; Kravets et al., 2019) are based on static particle arrangements, means that particle mobility is not taken into account. However, it is known that particle mobility has important effects on drag force, and this effect is even more important in low Reynolds numbers regime as particles are better able to alter the fluid flow around particles (Rosemann et al., 2021). Therefore, we also implemented a correlation that considers the effect of particle mobility (Tang et al., 2016). Comparing the correlation results for mobile and immobile particles, we have seen a significant deviation in the results which are becoming more obvious as closer to the wall and it shows the importance of particle mobility effect on both drag force and particle concentration profile near-wall.

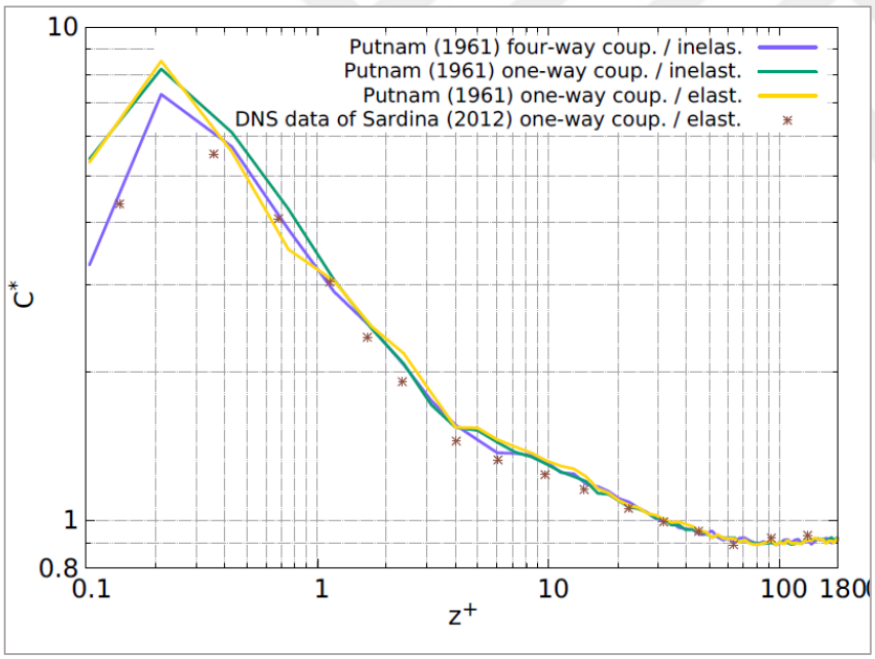

Figure 4.10. Influence of coupling approach and elasticity on the particle concentration profiles.

In Figure 4.10, we compared the simulation results of Sardina et al. (2012) with the results of our simulation for the case which we implemented Putnam's (1961) drag force correlation. We have observed very small differences in the concentration profile which occur in near-wall region and might be attributed to the

following reasons. Firstly, the drag force correlation used in the reference work is the Stokes drag correlation which is derived from the analytical solution to the Navier-Stokes equation and is strictly valid only for $Re_p \leq 1$. However, we employed Putnam's (1961) experimental correlation which is based on a fluid flowing around a static particle.

Secondly, in our simulation, four-way coupling approach is used means that the effect of particles on fluid, particle-particle and particle wall interactions are also taken into account. However, in the reference work, one-way coupling is implemented. In order to understand if the differences in the near-wall region is because of the coupling approach, we adjusted one-way coupling and ran the simulation again. However, we observed substantial differences in the near-wall region comparing the results with the Sardina et al.'s (2012) simulation results. Interestingly, our simulations with the one-way coupling approach deviates more from the Sardina et al.'s (2012) simulation results than our simulation results which four-way coupling is applied.

Thirdly, in our simulation collision of particles with the wall is inelastic (with the restitution coefficient of $\varepsilon = 0.9$), means that the kinetic energy on the particle is not conserved and is lost by internal frictions during collision with the wall. On the other hand, in the reference paper, purely elastic collisions are simulated. In elastic collisions, it is assumed that all kinetic energy is conserved and no energy is lost due to friction. From a previous DNS work, it has been reported that the difference between restitution coefficient of $\varepsilon = 0.9$ and $\varepsilon = 1$ does not change the simulation results (Li et al., 2001). However, in the simulation work mentioned, unlike our simulation setup, both the lift and gravity forces are taken into account. Therefore, in their simulation, the effect of restitution coefficient compared to lift and gravity forces might be negligible but it might be important in our simulations. In order to understand the effect of restitution coefficient in our simulations, we have performed a simulation case with purely elastic collisions. Differences between these two cases are found to be insignificant as it is reported in the paper mentioned, even in the absence of lift and gravity forces (Figure 4.10).

Finally, as well as differences in the modelling of simulations, inconsistency in the results can also be attributed to how the results are presented. In order to show the importance of post-processing, we used different arrangement and size of bins to present the simulation results (Figure 4.11). According to our simulation results, it is clear that the starting point and the number of the bins make significant differences in the concentration profile in the near-wall region. For example, at $z \cong 0.15$, when the first bin is at $z^+ = r$, our data point is very near to that of Sardina et al. (2012) and around $C^* = 4.3$. However, for the other case (first bin $z^+ = 0$), there is a significant deviation with $C^* \cong 5.9$ and $C^* \cong 6.5$ for 140 and 130 number of bins respectively. Therefore, it is also clear that number of bins make significant deviations in the concentration profile.

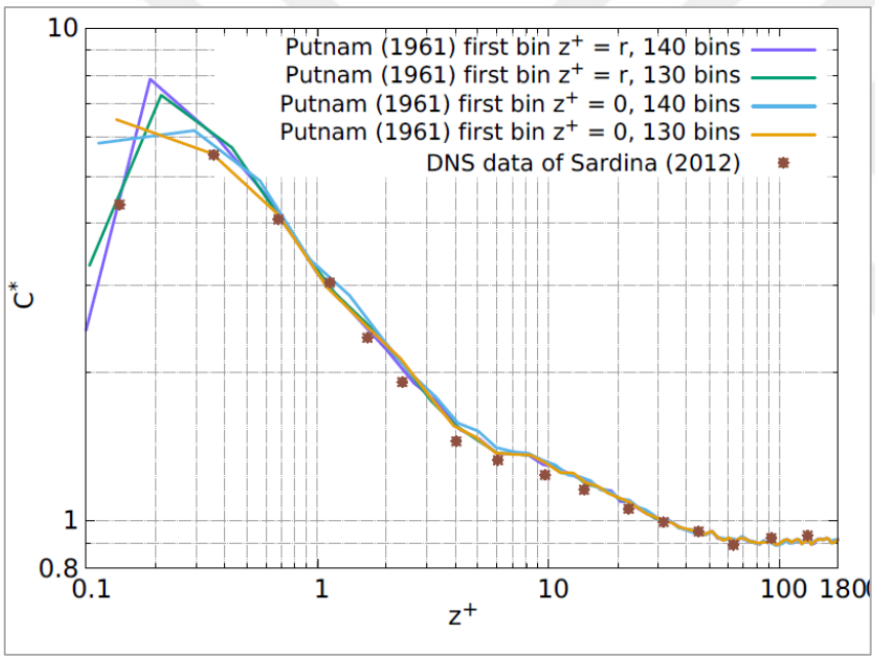

Figure 4.11. Influence of post-processing methods on particle concentration profiles.

In Figure 4.12, we showed the acceleration due to drag force with respect to normalized distance from the wall. Acceleration due to drag is normalized by the gravity (g = 9.81 m/s^2). It is seen that, the acceleration due to drag force is very low in the near-wall region compared to moderate distances from the wall. However, the implemented drag force correlations alter the particle concentration profile in the near-wall region. This situation can be explained as particle's backward, forward motions in the wall-normal direction. As a result of these motions, the

acceleration due to drag that a particle have at the moderate distances from the wall might affect the particle concentration in the near-wall region.

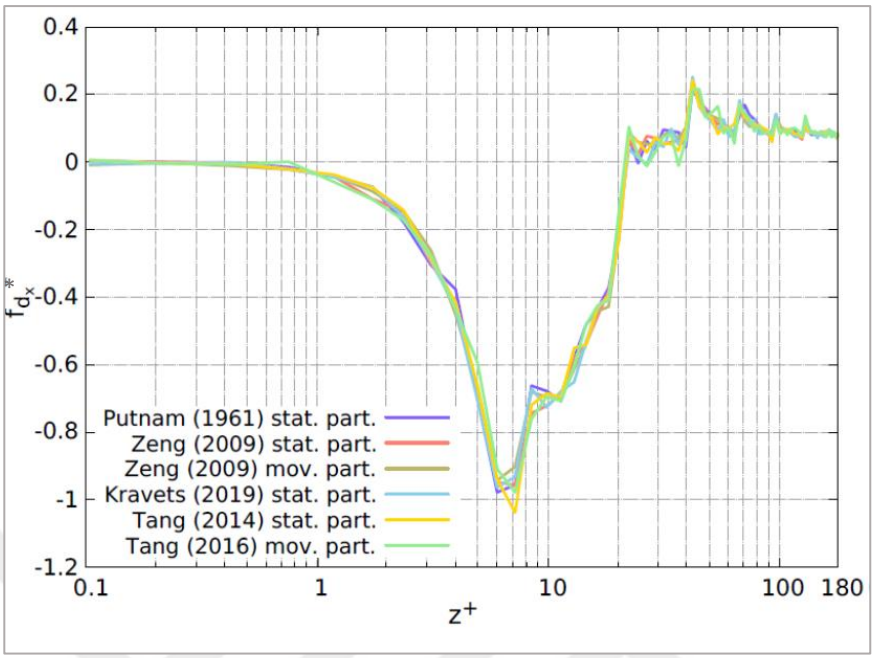

Figure 4.12. Acceleration due to drag force with respect to normalized distance from the wall using different drag force correlations for the uncharged particles. (Acceleration due to drag is normalized by the gravity force.)

4.2 Charged Particles

By far we investigated the simulation results for the uncharged particles. In the following we are going to look at; what is the general pattern of flow and what is the effect of drag force modelling on the particle and fluid dynamics for the charged particles.

4.2.1 Temporal Evolution of Particle Concentration of Charged Case

In Figure 4.12 a couple of temporal evolution (history) of concentration profile in the region nearest to the wall for charged particles ($q_1 = 1 \times 10^{-16}$ C and $q_2 = 1 \times 10^{-15}$ C) using Putnam (1961)'s correlation is given. In our simulations, all particles have the same charge, and the charge of the particles does not change with time. In physical terms, it means that we neglected the charge exchange as a result of particle-particle, particle-wall collisions. For the charged case we started

the simulations where uncharged case has reached steady-state which is about 38 seconds.

It is seen that, when particles have the electric charge of q_2, particle concentration in the near-wall region even more increases. On the other hand, for the case which particles have the charge of q_1, there is still small increase in the concentration in the near-wall region. However, this increase is not as obvious as in the case which particles have higher charges.

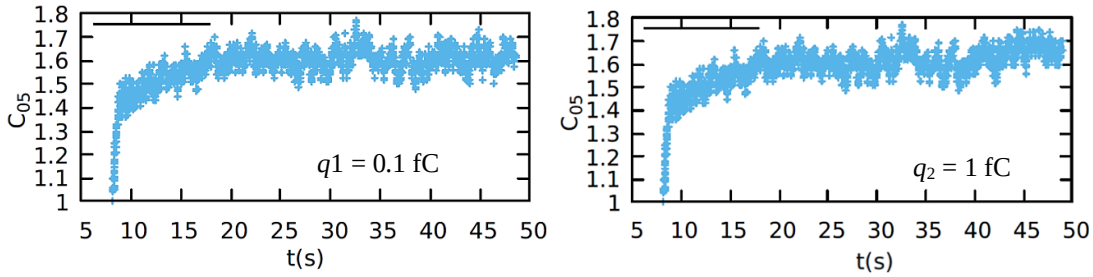

Figure 4.12. Temporal evolution of particle concentration in the 5% of the channel closest to the wall for charged cases using Putnam's (1961) drag correlation.

4.2.2 Results of Simulations for Charged Case

In Figure 4.13 we showed particle Reynolds number with respect to normalized distance from the wall using Putnam's (1961) drag force correlation. Results of the other simulations have small deviations, but also have the same pattern, so that we only showed the results of one correlation to examine the general pattern. As it is for the uncharged case, particle Reynolds number is in the range of $Re_{\mathrm{p}} < 0.1$. Also, particle Reynolds number is low in the near wall region and increases moving away from the wall.

Comparing the results of different charge levels, it is seen that there is a decrease in the particle Reynolds number with the increase in the electrostatic charge of particles. However, this effect is only seen in the region of ($z^+ \ll 0.2$). For the charged cases, similar to uncharged case, increase in the particle Reynolds number up to ($z^+ = 13$) is seen. Also, approaching the center particle Reynolds

number decrease dramatically for both charged and uncharged cases as a result of decrease in relative velocity (Figure 4.14)

In Figure 4.14, relative velocity of particles with respect to normalized distance from the wall is given. Here, we normalized relative velocity with the wall friction velocity ($u_\tau = 0.1314$). We have seen that, relative velocitiy profiles have the same pattern for the uncharged and charged case, however, deviations using different correlations observed mostly in the region $3 < z^+ < 20$.

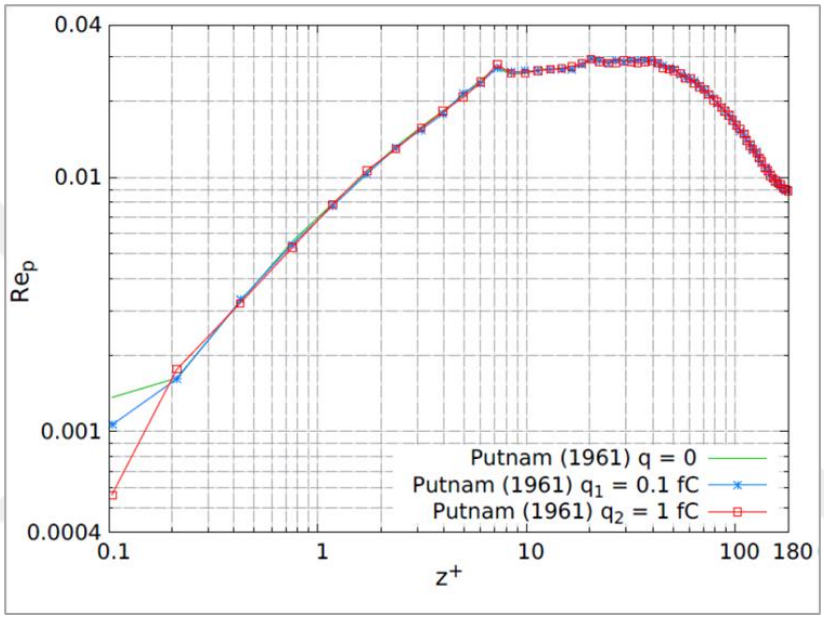

Figure 4.13. Particle Reynolds number with respect to normalized difference from the wall for charged and uncharged cases using drag force correlation of Putnam (1961).

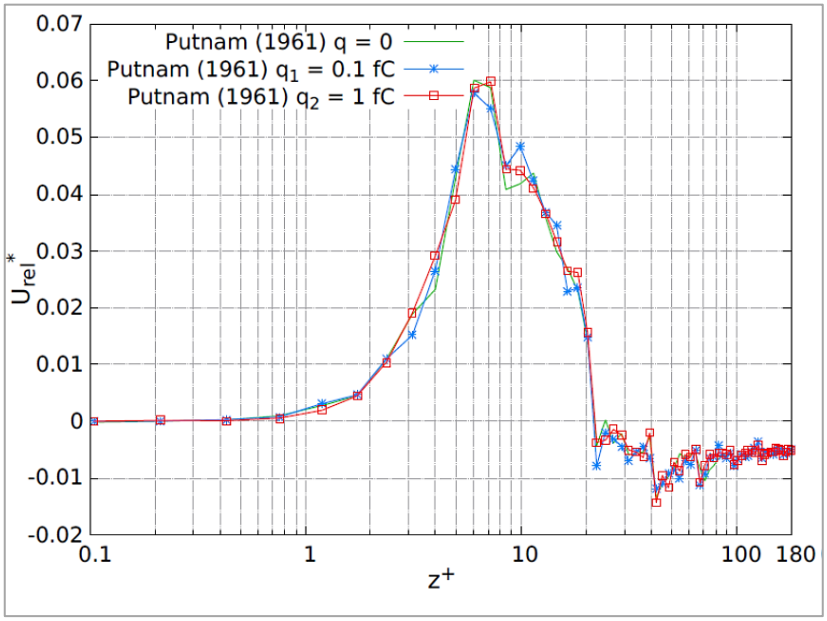

Figure 4.14. Relative velocity of particles with respect to normalized difference from the wall for charged and uncharged cases using drag force correlation of Putnam (1961).

In the previous section, we discussed the tendency of uncharged particles to be at lower turbulence energy levels due to the effect of turbophoresis, resulting in their deposition near the wall. In order to check the preferential accumulation region of the charged particles, we looked at particle concentration profiles using different drag force correlations and for different charge levels in Figure 4.16.

Comparing the concentration profiles for the uncharged and charged particles, it is observed that the particle concentration is higher for the charged case in the near-wall region compared to uncharged case. Also, particles' tendency to accumulate on the wall increase with the increasing the charge of the particles. On the other hand, the electric field that the particles create is proportional to number of particles in that region. As a result of higher particle concentrations, the effect of charge of particles on concentration profile only exist in the near-wall region.

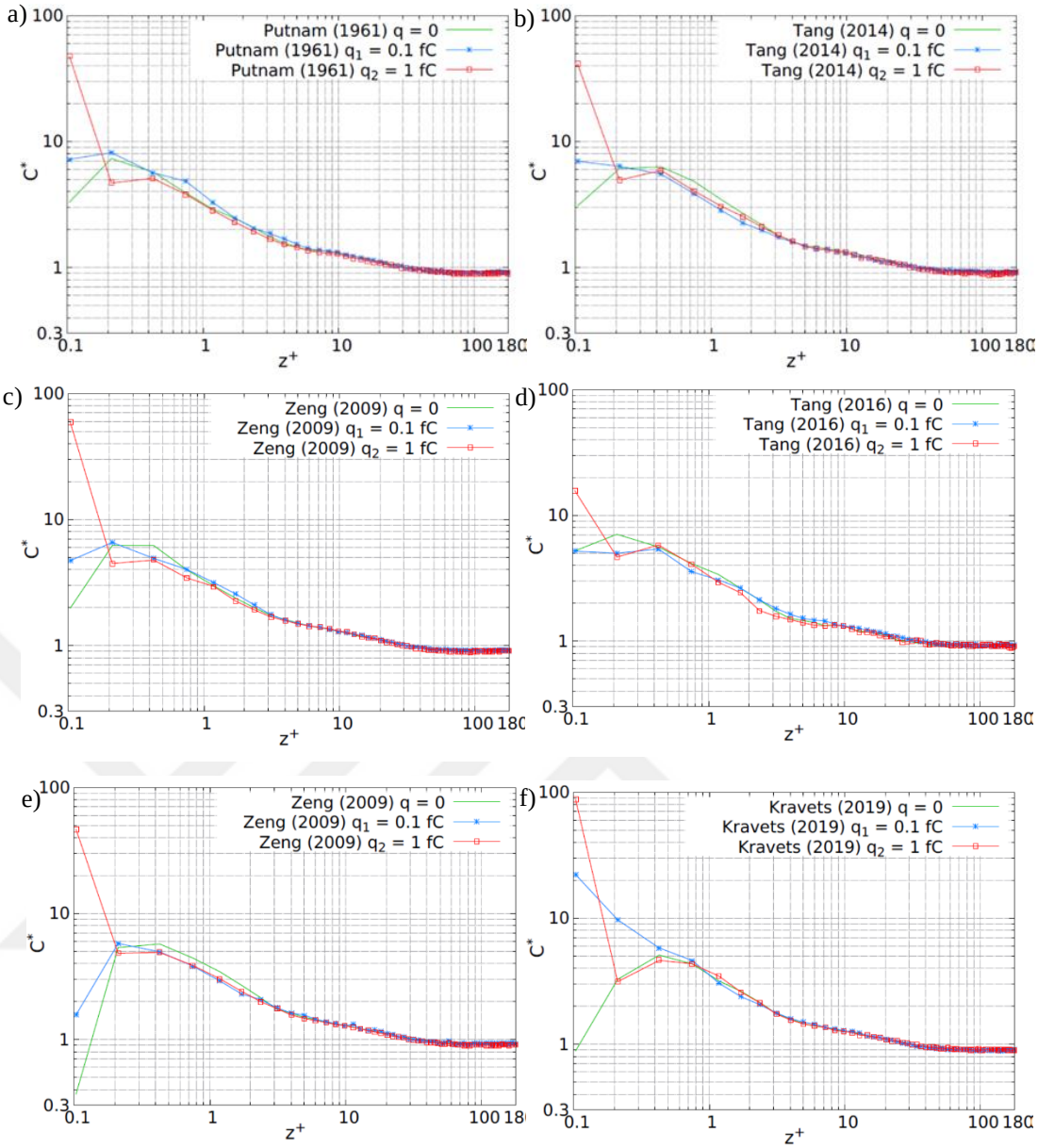

Figure 4.15. Concentration profiles using different drag force correlations for charged and uncharged cases (b) is the concentration profile using Zeng et al.'s (2009) correlation for stationary particles and c) for moving particles.

Looking at the general pattern for the charged particles with the charge of q_2, it is seen that the accumulation region of the particles shifts directly to the wall. The reason of this phenomena is that, instead of accumulating in the near-wall region due to the effect of turbophoresis, for sufficienlty charged particles, electric forces dominate the effect of turbophoresis, and push the particles directly to the wall. On the other hand, particles which are going back to the bulk flow with the effect of turbulence diffusion are prevented by the electric forces in the opposite direction. Acceleration due to electric field with respect to normalized distance from the wall

is given in Figure 4.16 and Figure 4.17 It is seen that acceleration due to electric field increases approaching the wall. This increase is related to increase in particle concentration approaching the wall. On the other hand, a small decrease in the particle concentration at the wall is seen for the charge level q_2.

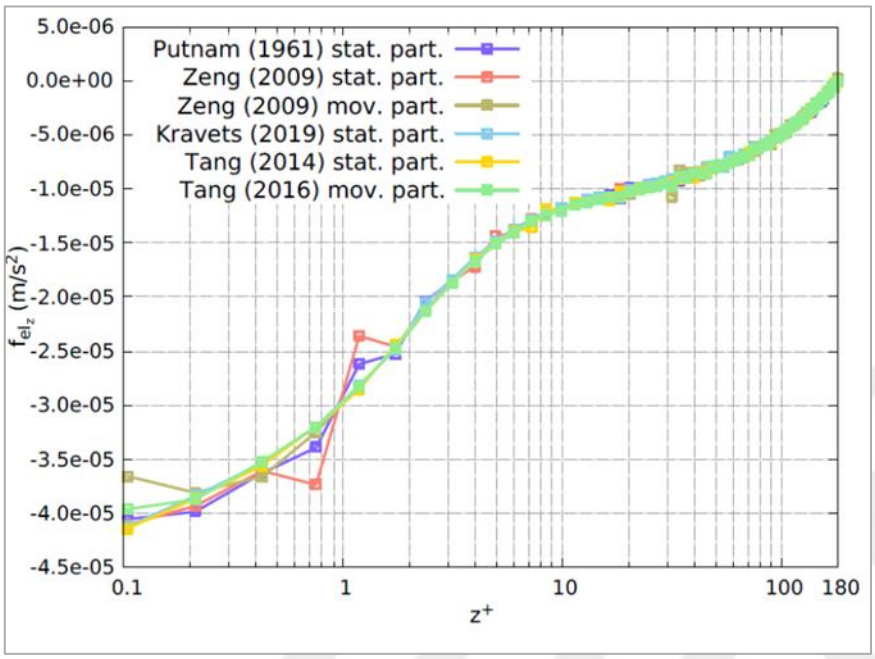

Figure 4.16. Acceleration due to electric field with respect to normalized distance from the wall for the charge level q_1

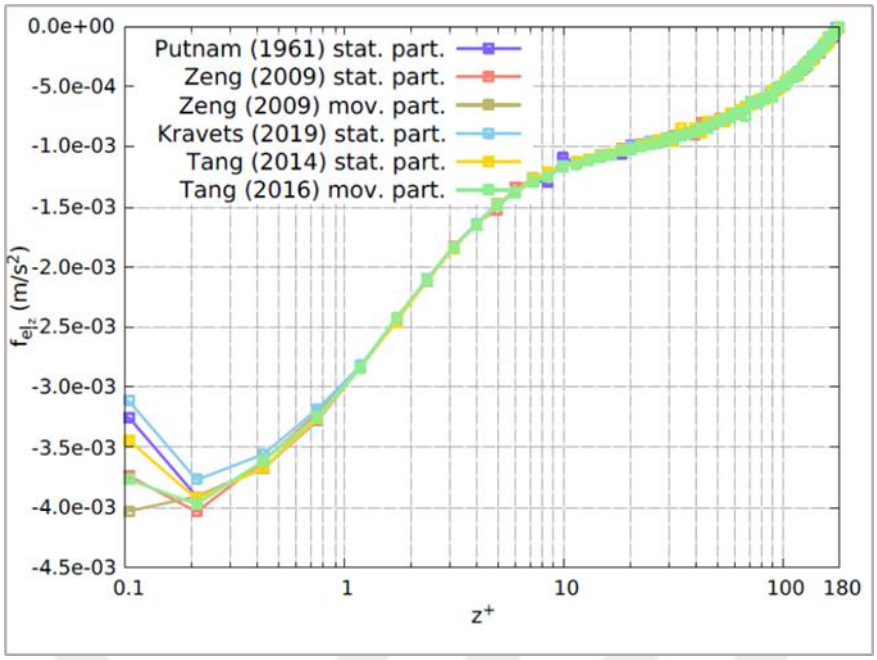

Figure 4.17. Acceleration due to electric field with respect to normalized distance from the wall for the charge level q_2

Grosshans et al. (2018) reported that, as a result of deposition of particles at the wall, charged particles pushed the other particles out of the deposition region at the wall, and tend to smoothen the particle concentration curve. However, we did not observe the smoothening effect of the repelling forces in our simulations. As it is already discussed in the paper mentioned, the reason of not seeing the smoothing effect of repelling forces can be attributed to the level of electric field. Electric field is created by the electrically charged particles. Therefore, in our simulation, particles might not have enough charge or particle concentration might not be high enough to create an electric field that is able to push out the particles from the wall.

Comparing the results of different drag force correlations for different charge levels, we saw that the closures that consider the effect of a near-wall (Zeng et al., 2009) have very similar results with each other and also with the correlation of (Putnam, 1961) for the particles with the charge of q_2. Also, deviations for the correlations considering the surrounding particles (Tang et al., 2014; Tang et al., 2016; Kravets et al., 2019) reduced as the charge increased but still, more than the closures for the wall-effect. However, this situation is only valid for particle charge of q_2, as the results using different drag force correlations for the particles with charge q_1 are different in the near-wall region. Therefore, when the particles

charged enough, (in our case it is $q_2 = 1 \times 10^{-15}$ C), due to the dominance of electric forces, drag force modelling becomes less significant.

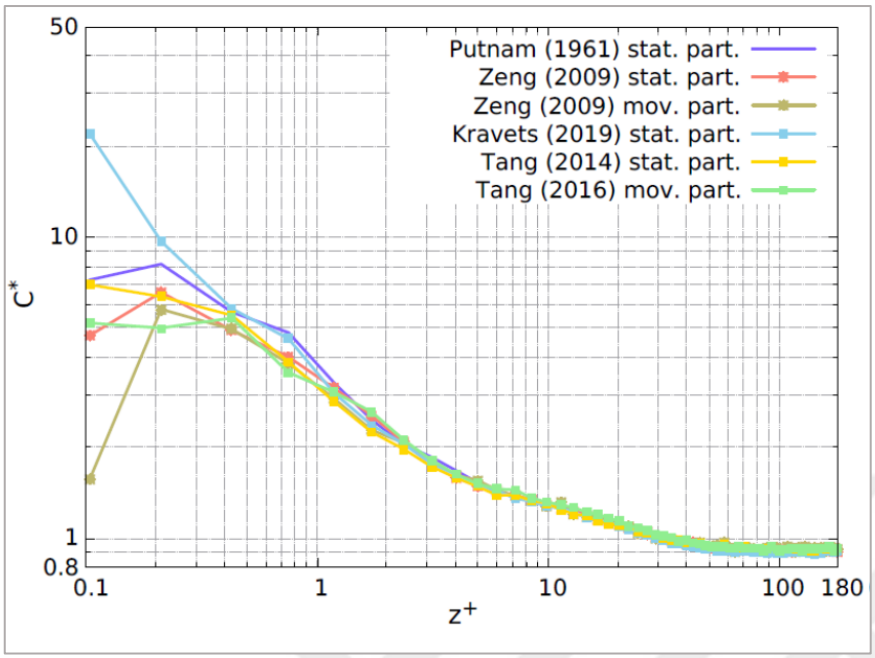

Figure 4.18. Particle concentration profiles for the charge level q_1

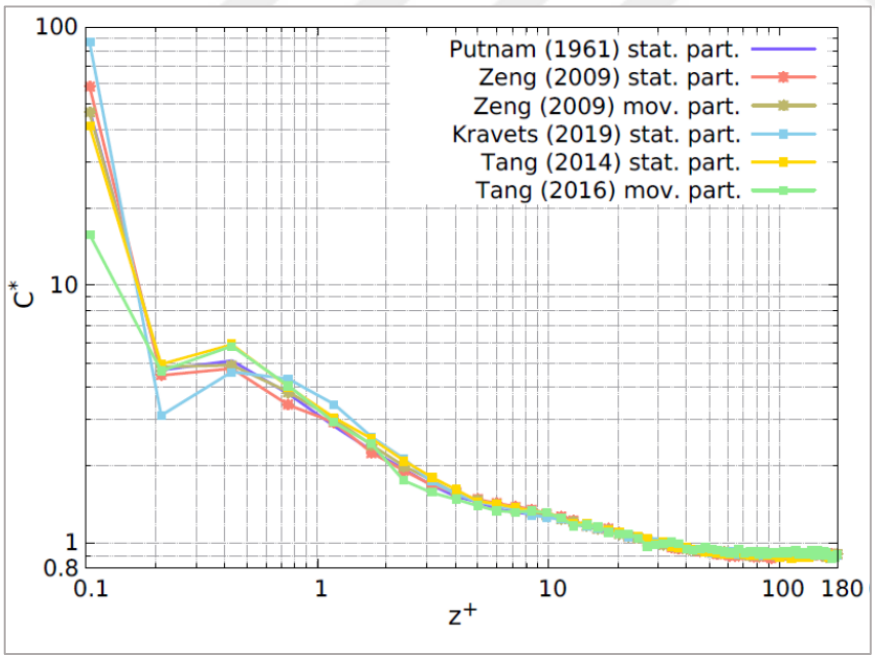

Figure 4.19. Particle concentration profiles for the charge level q_2

5 CONCLUSION

Our study is concluded in three main parts which we investigate the general properties of simulations, the effect of post-processing on the simulation results, and drag force modeling for charged and uncharged cases separately.

5.1 Common Properties of the Simulations

It is seen in our simulations that, for all simulation cases (charged and uncharged) Re_{p} is lower than 0.1 means that we have Stoke's flow regime. We have seen the effect of turbophoresis in our simulations, which results in the accumulation of particles in the near wall region $0.1 \leq z^{+} \leq 0.5$. On the other hand, for sufficiently charged particles ($q_2 = 1 \times 10^{-15}$ C) accumulation region shifted directly to the wall. Therefore, for the charged case, long-term accumulation of particles in that specific region due to effect of turbophoresis is dominated by the electric field that is created by the charged particles. We have also seen that; the effect of electric field is to increase the particle concentration at the wall.

5.2 Effect of Post-Processing Method on Simulation Results

Different arrangement and size of bins are used to investigate the importance of post-processing method. We obtained deviations in the concentration profile (only in the near-wall region) using different number, and starting point of bins. Therefore, it is clear that post-processing method makes significant differences in the concentration profile in the near-wall region and in order to quantitatively compare simulation results, they should be clearly defined.

5.3 Drag Force Modelling

Comparing the results of different simulation cases, it is seen that;

- particle concentration profiles we obtained using different drag force models are different for the uncharged case in the near wall region ($z = 5^{+}$),

- however, at moderate distances from the wall, the results obtained using different correlations are becoming the same $z^+ \geq 5$,

- due to higher particle concentration and non-uniformity in the near-wall region, consideration of other particles on drag force is important,

- due to non-uniformity that the wall creates, consideration of presence of a nearby-wall on drag force is important,

- correlations for the presence of a nearby-wall, have the same pattern, which is to reduce the particle concentration in the near-wall region,

- a general trend for the correlations that considers the effect of other particles has not been observed,

- consideration of particle mobility on drag force is found to be important, for example; concentration profile we obtained using Tang et al.'s (2014) study which is obtained based on static particle arrangements, is different from Tang et al.'s (2016) study based on mobile particles,

- when the particles sufficiently charged (in our case it is $q_2 = 1 \times 10^{-15}$ C), due to dominance of electric field, effect of drag force modelling on the particle concentration is low.

Therefore, for the uncharged particles, drag force modelling is important in the near-wall region, and above $z^+ \cong 5$ it might be insignificant. Correlations consider the effect of a nearby-wall have the same pattern on the concentration profile, therefore we propose to use Zeng et al.'s correlations. For the charged particles, when the electric charge of the particles increases, electric forces dominate the drag force, and it means that, for higher charge levels, drag force modelling might be insignificant. However, we should note that, this situation is only valid for our limited physical conditions (very low Reynolds numbers $Re_{\mathrm{p}} \ll 1$, very dilute flow) and might be different for any other cases.

ACKNOWLEDGEMENT

Firstly, I would like to express my deepest gratitude to my supervisors Prof. Dr. Mustafa DEMIRCIOGLU and PD Dr. habil Holger GROSSHANS for their invaluable assistance and support.

I would like to thank the Physikalisch-Technische Bundesanstalt (PTB) for allowing me to access their computational labs.

My sincere thanks go to Prof. Dr. Uwe KLAUSMEYER for providing me an opportunity to make an internship in PTB which then turned into this master thesis.

Finally, I am very grateful to my family for their continuous supports all my life.

This project has received funding from the European Research Council (ERC) under the European Union's Horizon 2020 research and innovation programme (grant agreement No. 947606 PowFEct).

Gizem ÖZLER

IZMIR

09/01/2022

REFERENCES

Beetstra, R., van der Hoef, M.A. and Kuipers, J.A.M., 2007, Drag force of intermediate Reynolds number flow past mono and bidisperse arrays of spheres, *AIChE Journal*, 53(2):489–501 pp.

Benyahia, S., Syamlal, M. and O'Brien, T., 2006, Extension of Hill-Koch-Ladd drag correlation over all ranges of Reynolds number and solids volume fraction, *Powder Technology*, 162:166-174 pp.

Bi, Q., 2015, Numerical Modelling of Near-bottom Sediment Transport: Turbulence Modulation, New Process Models and Application to the Scheldt and Belgian Coast. PhD dissertation, Dept. of Civil Engineering, KU Leuven, 228 pp.

Bissinger, C., and Grosshans, H., 2020, A new computational algorithm for the interaction between electrically charged particles, *SN Applied Sciences*, 2(5): 1-10 pp.

Brauer, H. and Mewes, D., 1972, Strömungswiderstand sowie stationaer und instationare Stoff- und Warmeübergang an Kugeln, *Chem Ing Tech*, 44:865-868 pp.

Carman, P.C., 1956, Flow of gases through porous media. Butterworths, London

Chorin, A. J., Marsden, J. E. and Marsden, J. E., 1990, A mathematical introduction to fluid mechanics, New York: Springer-Verlag. 47 pp.

Clift, R., Gauvin, W.H., 1970, The motion of particles in turbulent gas streams, *In Proc. Chemeca*, 70:14–28 pp.

Crowe, C., Schwarzkopf, J. D., Sommerfeld, M. and Tsuji, Y., 2012, Multiphase Flows with Droplets and Particles (2nd ed.), CRC Press, Boka Raton, 250p.

Dallavalle, J. M., 1948, Micromeritics: the technology of fine particles.

REFERENCES (continued)

Di Felice, R., 1994, The voidage function for fluid-particle interaction systems, *International Journal of Multiphase Flow*, 20(1):153-159 pp.

Ergun, S. and Orning, A. A., 1949, Fluid flow through randomly packed columns and fluidized beds, *Ind. Eng. Chem.*, 41:1179–1184 pp.

Faxén , H., 1922, Der Widerstand gegen die Bewegung einer starren Kugel in einer zähen Flüssigkeit, die zwischen zwei parallelen ebenen Wänden eingeschlossen ist, *Annalen der Physik*, 373(10):89–119 pp.

Gidaspow, D., 1994, Multiphase Flow and Fluidization: Continuum and Kinetic Theory Description, Academic Press, San Diego, CA.

Gilbert, M., Davis, L. and Altman, D., 1955, Velocity lag of particles in linearly accelerated combustion gases, *Jet Propulsion*, 25:26–30 pp.

Gobin, A., Neau, H., Simonin, O., Llinas, J. R., Reiling, V., and Sélo, J. L., 2003, Fluid dynamic numerical simulation of a gas phase polymerization reactor. *International journal for numerical methods in fluids*, *43*(10-11), 1199-1220 pp.

Goldman, A. J., Cox, R. G. and Brenner, H., 1967a, Slow viscous motion of a sphere parallel to a plane wall—I Motion through a quiescent fluid. *Chemical Engineering Science*, 22(4):637–651 pp.

Goldman, A. J., Cox, R. G., and Brenner, H., 1967b, Slow viscous motion of a sphere parallel to a plane wall—II Couette flow. *Chemical engineering science*, 22(4):653-660 pp.

Goldstein, S., 1929, The steady flow of viscous fluid past a fixed spherical obstacle at small Reynolds numbers, *Proceedings of the Royal Society of London*, 123:225–235 pp.

REFERENCES (continued)

Goossens, W., 2019, Review of the empirical correlations for the drag coefficient of rigid spheres, *Powder Technology*, 352:350-359 pp

Grosshans, H. and Papalexandris, M., 2017, Direct numerical simulation of triboelectric charging in particle-laden turbulent channel flows, *Journal of Fluid Mechanics*, 818:465-491 pp.

Grosshans, H., Bissinger, C., Calero, M., and Papalexandris, M. V., 2021, The effect of electrostatic charges on particle-laden duct flows. *Journal of Fluid Mechanics*, 909.

Grosshans, H., Villafañe, L., Banko, A., and Papalexandris, M. V., 2018, Influence of electrostatic charges on the particle concentration in wall-bounded turbulent flows. In *8th World Congress on Particle Technology*, Orlando, FL, USA.

Hill, R.J., Koch, D.L. and Ladd, J.C., 2001a, Moderate-Reynolds-numbers flows in ordered and random arrays of spheres, *Journal of Fluid Mechanics*, 448:243–278 pp.

Hill, R.J., Koch, D.L. and Ladd, J.C., 2001b, The first effects of fluid inertia on flows in ordered and random arrays of spheres, *Journal of Fluid Mechanics*, 448:213-241 pp.

Hoef, M., Beetstra, R., and Kuıpers, J., 2005, Lattice-Boltzmann simulations of low-Reynolds-number flow past mono- and bidisperse arrays of spheres: results for the permeability and drag force, *Journal of Fluid Mechanics*, 528:233-254 pp.

Kozeny, J., 1927, Ueber kapillare Leitung des Wassers im Boden, *Sitzungsber Akad. Wiss.*, 136(2a):271-306

REFERENCES (continued)

Kravets, B., Rosemann, T., Reinecke, S. and Kruggel-Emden, H., 2019, A new drag force and heat transfer correlation derived from direct numerical LBM-simulations of flown through particle packings, *Powder Technology*, 345 pp.

Lapple, C. E. and Shepherd, C. B., 1940, Calculation of Particle Trajectories, *Ind. Eng. Chem.*, 32:605-617 pp.

Li, Y., McLaughlin, J. B., Kontomaris, K., and Portela, L., 2001, Numerical simulation of particle-laden turbulent channel flow, *Physics of Fluids*, 13(10): 2957-2967 pp.

Liao, S., 2002, An analytic approximation of the drag coefficient for the viscous flow past a sphere, *International Journal of Non-Linear Mechanics*, *37*(1):1-18 pp.

Mallouppas, G., and van Wachem, B., 2013, Large Eddy Simulations of turbulent particle laden channel flow, *International Journal of Multiphase Flow*, 54:65-75 pp.

Marchioli, C., and Soldati, A., 2002, Mechanisms for particle transfer and segregation in a turbulent boundary layer, *Journal of fluid Mechanics*, 468:283-315 pp.

Matsusaka, S., Maruyama, H., Matsuyama, T., and Ghadiri, M., 2010, Triboelectric charging of powders: A review, *Chemical Engineering Science*, 65(22):5781-5807 pp.

Oseen, C. W., 1910, Über die Stokes'sche Formel und über eine verwandte Aufgabe in der Hydrodynamik. Ark. *Mat., Astron. och Fys*. 9(29).

Peskin, C. S., 2002, The immersed boundary method, *Acta numerica*, 11:479-517 pp.

REFERENCES (continued)

Picciotto, M., Marchioli, C., Reeks, M. W., and Soldati, A., 2005, Statistics of velocity and preferential accumulation of micro-particles in boundary layer turbulence. *Nuclear engineering design*, *235*(10-12):1239-1249 pp.

Proudman, L., Pearson, J. R., 1957, Expansion at small Reynolds number for the flow past a sphere and a circular cylinder, *Journal of Fluid Mechanics,* 2:237–262 pp.

Putnam, A., 1961, Integratable Form of Droplet Drag Coefficient., *ARS J.*, 31:1467-68 pp.

Rosemann, T., Reinecke, S. R., & Kruggel-Emden, H., 2021, Analysis of Mobility Effects in Particle-Gas Flows by Particle-Resolved LBM-DEM Simulations. *Chemie Ingenieur Technik*, 93(1-2): 223-236 pp.

Sardina, G., Schlatter, P., Brandt, L., Picano, F. and Casciola, C., 2012, Wall accumulation and spatial localization in particle-laden wall flows, *Journal of Fluid Mechanics*, 699: 50-78 pp.

Schiller, L., Nauman, A.Z., 1933, Uber die grundlengenden berechungen bei schwerkraftaufbere-itung. *Zeitschrift des Vereines Deutscher Ingenieure*, 77:318-320 pp.

Stokes, G. G., 1851, On the effect of internal friction of fluids on the motion of a pendulum, *Trans. Cambridge Phil. Soc.*, 9:8

Tabaeikazerooni, S. H., 2019, Laminar and turbulent particle laden flows: a numerical and experimental study (Doctoral dissertation, KTH Royal Institute of Technology).

Tang, Y., Peters, E., Kuipers, J., Kriebitzsch, S., and van der Hoef, M., 2014, A new drag correlation from fully resolved simulations of flow past monodisperse static arrays of spheres, *Aiche Journal*, 61(2): 688-698 pp.

REFERENCES (continued)

Tang, Y., Peters, E., and Kuipers, J., 2016, Direct numerical simulations of dynamic gas-solid suspensions, *AiChE Journal*, 62(6):1958–1969 pp.

van der Hoef, M. A., Beetstra, R., and Kuipers, J. A. M., 2005, Lattice-Boltzmann simulations of low-Reynolds-number flow past mono-and bidisperse arrays of spheres: results for the permeability and drag force, *Journal of fluid mechanics*, 528:233-254 pp.

Wen, C. Y. and Yu, Y. H., 1966, Mechanics of fluidization. In Chem. Eng. Prog. Symp. Ser., 62: 100-111 pp.

Zeng, L., Najjar, F., Balachandar, S. and Fischer, P., 2009, Forces on a finite-sized particle located close to a wall in a linear shear flow, *Physics of fluids*, 21(3), 033302

CURRICULUM VITAE

Gizem Özler

EDUCATION

University (MSc.):	(Izmir/TURKEY) Ege University (2019-), Chemical Engineering Department
University (BSc.):	(Izmir/TURKEY) Ege University (2014-June 2019), Chemical Engineering Department

PROJECTS

MSc. Thesis student in Physikalisch-Technische Bundesanstalt (Working group: Analysis and Simulation in Explosion Protection)
Braunschweig / GERMANY (01/2020 -)
Project name: Drag Force Modelling on the Flow of Charged Particles

- Improve the accuracy of pafiX simulations code by implementing a new drag force correlation.
- Investigate the effect of drag force modelling on the flow of charged particles.

Tubitak 2209-B Project in Kansai Altan Boya Sanayi A.Ş Kemalpaşa / IZMIR (10/2018 - 05/2019)
Project name: Wet Grinding Parameters in the Optimization of Nanoscale Calcite Production

- Experimental and computational study on the production of nanoscale calcite in acrylic resin. A code developed to find the parameters in population balance equations.

EXPERIENCES

Internship in Physikalisch-Technische Bundesanstalt – Braunschweig/GERMANY (01/2020 – 02/2020)
Department: Working Group 3.51 - Analysis and Simulation of Explosion Protection

- Studied direct numerical simulation of triboelectric charging in particle-laden turbulent channel flows through numerical programs

Summer Training in Group Farma -
Sancaktepe/ISTANBUL (07/2018 - 08/2018) Department:
RD Lab and Pilot Plant

- Studied on pharmaceutical drugs, manufacturing methods, quality control devices, all equipment that are used in the production department.
- Performed mass and energy balance on dryer.

Summer Training in Dyo Boya Fabrikaları A. Ş. -
Çiğli/IZMIR (07/2017 - 08/2017) Department: Synthetic Binder Production

- Performed mass and energy balance calculations on the reactor and heat exchanger with the consultation of responsible engineer.

SKILLS

Computer Skills:	Operating Systems (Ubuntu, Windows), MS Office programs (Word, Excel, PowerPoint, Visio.), Simulation software (Comsol Multiphysics, AspenTech), Computer programming (Fortran, MATLAB), Data analysis (Minitab), Computer- aided design (AutoCAD)
Language:	English (advanced), German (medium)

ACADEMIC REFERENCES

- Prof. Dr. Mustafa DEMIRCIOGLU

email: md.che.tr@gmail.com, mustafa.demircioglu@ege.edu.tr

- PD Dr. habil Holger GROSSHANS

email: holgergrosshans@ptb.de

APPENDIX A

- **Non-dimensionalization of Navier Stokes Equation**

The incompressible, dimensional Navier-Stokes equation without body forces is given below:

$$\frac{\partial \boldsymbol{u}}{\partial t} + (\boldsymbol{u} \cdot \boldsymbol{\nabla})\boldsymbol{u} = -\frac{1}{\rho_{\mathrm{f}}}\boldsymbol{\nabla} P + v\boldsymbol{\nabla}^2\boldsymbol{u}$$

The equation above is non-dimensionalized by replacing the dimensional variables with non-dimensional variables. In order to do that, dimensional variables are divided by the appropriate characteristic scales.

For the turbulent wall-bounded flows, it is common to use the friction Reynolds number, Re_τ, which is calculated as '$Re_\tau = u_\tau \delta / v$' so that the characteristic velocity scale is the wall friction velocity, u_τ and the characteristic length scale is the channel half-width, δ. Accordingly, the non-dimensional variables are computed as; non-dimensional time $t^* = t u_\tau / \delta$, non-dimensional velocity $\boldsymbol{u}^* = \boldsymbol{u}/u_\tau$, non-dimensional distance from the wall, $y^* = y/\delta$, non-dimensional pressure, $P^* = P/\rho u_\tau^2$ (also $\boldsymbol{\nabla}^* = \delta \boldsymbol{\nabla}$ and $\boldsymbol{\nabla}^{*2} = \delta^2 \boldsymbol{\nabla}^2$). Placing the new terms to Navier-Stokes equation gives non-dimensional Navier-Stokes equation:

$$\frac{\partial \boldsymbol{u}^*}{\partial t^*} + \boldsymbol{u}^* \cdot \boldsymbol{\nabla}^* \boldsymbol{u}^* = -\boldsymbol{\nabla}^* P^* + \frac{1}{Re_\tau}\boldsymbol{\nabla}^{*^2}\boldsymbol{u}^*$$

and the corresponding x-momentum balance equation:

$$\frac{\partial u^*}{\partial t^*} + u^*\frac{\partial u^*}{\partial x^*} + v^*\frac{\partial u^*}{\partial y^*} + w^*\frac{\partial u^*}{\partial z^*} = -\frac{\partial P^*}{\partial x^*} + \frac{1}{Re_\tau}\left(\frac{\partial^2 u^*}{\partial x^{2^*}} + \frac{\partial^2 u^*}{\partial y^{2^*}} + \frac{\partial^2 u^*}{\partial z^{2^*}}\right)$$

We assumed that the fluid flow is fully-developed, steady-state and only in x-direction so that;

-fully developed flow: $\frac{\partial u^*}{\partial x^*} = 0$

- steady-state: $\frac{\partial u^*}{\partial t^*} = 0$

- only in x-direction: $v^* = w^* = 0$

We have a uniform pressure gradient that drives the flow so that $\frac{\partial P^*}{\partial x^*}$ is a constant. With the given simplifications, final form of the x-momentum equation is given as:

$$\frac{\partial P^*}{\partial x^*} = \frac{1}{Re_\tau}\left(\frac{\partial^2 u^*}{\partial z^{2^*}}\right)$$

We can calculate the wall friction velocity, u_τ, from $Re_\tau = u_\tau \delta/\nu$ for '$Re_\tau = 180$'. In our simulation half-width of the channel and kinematic viscosity of the fluid are 0.02 m and 1.46×10^{-5} m^2/s respectively. So, the wall friction velocity is $u_\tau = 0.1314$ m/s.

The wall friction velocity can be defined as $u_\tau = \sqrt{\tau_w/\rho_f}$, where τ_w is the shear rate at the surface of the wall. From here, τ_w is calculated as 0.0207.

By using τ_w, we can compute $\frac{\partial u}{\partial z}$ at the surface of the wall where the dynamic viscosity of the fluid is equal to 1.752×10^{-5}.

$$\tau_w = \mu \frac{\partial u}{\partial z}\Big|_{z=\pm\delta}$$

$$0.0207 = (1.752 \times 10^{-5}) \frac{\partial u}{\partial z}\Big|_{z=\pm\delta}$$

$$\frac{\partial u}{\partial z}\Big|_{z=\pm\delta} = 1181.51$$

In order to use the nondimensional Navier-stokes equation we can use characteristic scales:

$$\left.\frac{\partial u}{\partial z}\right|_{z=\pm\delta} = \frac{u_\tau}{\delta}\left.\frac{\partial u^*}{\partial z^*}\right|_{z^*=\pm 1}$$

$$\left.\frac{\partial u^*}{\partial z^*}\right|_{z^*=\pm 1} = 179.83$$

- **Boundary Conditions**

BC.1: Maximum fluid velocity at the center of the channel:

$$z = 0\ ;\ \frac{\partial u}{\partial z} = 0$$

$$z^* = 0\ ;\frac{\partial u^*}{\partial z^*} = 0$$

BC.2: No-slip at the wall:

$$z = \pm\delta;\ u = 0$$

$$z^+ = \pm 1\ ;\ u^+ = 0$$

B.C.3: Wall shear:

$$z = \pm\delta; \quad \tau_w = \mu\frac{\partial u}{\partial z}$$

$$z^+ = \pm 1; \quad \frac{\partial u^*}{\partial z^*} = 179.83$$

Applying the boundary conditions to the nondimensional x-momentum equation:

B.C.1:

$$\frac{\partial^2 u^+}{\partial z^{2+}} = Re_\tau \frac{\partial P^+}{\partial x^+}$$

$$\frac{\partial u^+}{\partial z^+} = Re_\tau \frac{\partial P^+}{\partial x^+} z^+ + c_1$$

$$z^+ = 0\,; \frac{\partial u^+}{\partial z^+} = 0 \longrightarrow c_1 = 0$$

$$\frac{\partial u^+}{\partial z^+} = Re_\tau \frac{\partial P^+}{\partial x^+} z^+ + c_1 \longrightarrow \frac{\partial u^+}{\partial z^+} = Re_\tau \frac{\partial P^+}{\partial x^+} z^+$$

B.C.3: Given the shear rate at the wall (for $Re_\tau = 180$):

$$z = \pm\delta; \quad \tau_w = \mu \frac{\partial u}{\partial z} \longrightarrow z^* = \pm 1; \quad \frac{\partial u^*}{\partial z^*} = 179.83$$

$$\frac{\partial P^+}{\partial x^+} = \frac{\partial u^+}{\partial z^+} \frac{Re_\tau}{z^+}$$

$$\frac{\partial P^+}{\partial x^+} = 0.999$$

Calculating the dimensional pressure gradient:

$$\frac{\partial P}{\partial x} = \frac{\rho_f {u_\tau}^2}{\delta} \frac{\partial P^+}{\partial x^+}$$

$$\frac{\partial P}{\partial x} = -1.035 \text{ (N/m}^3\text{)}$$

APPENDIX B

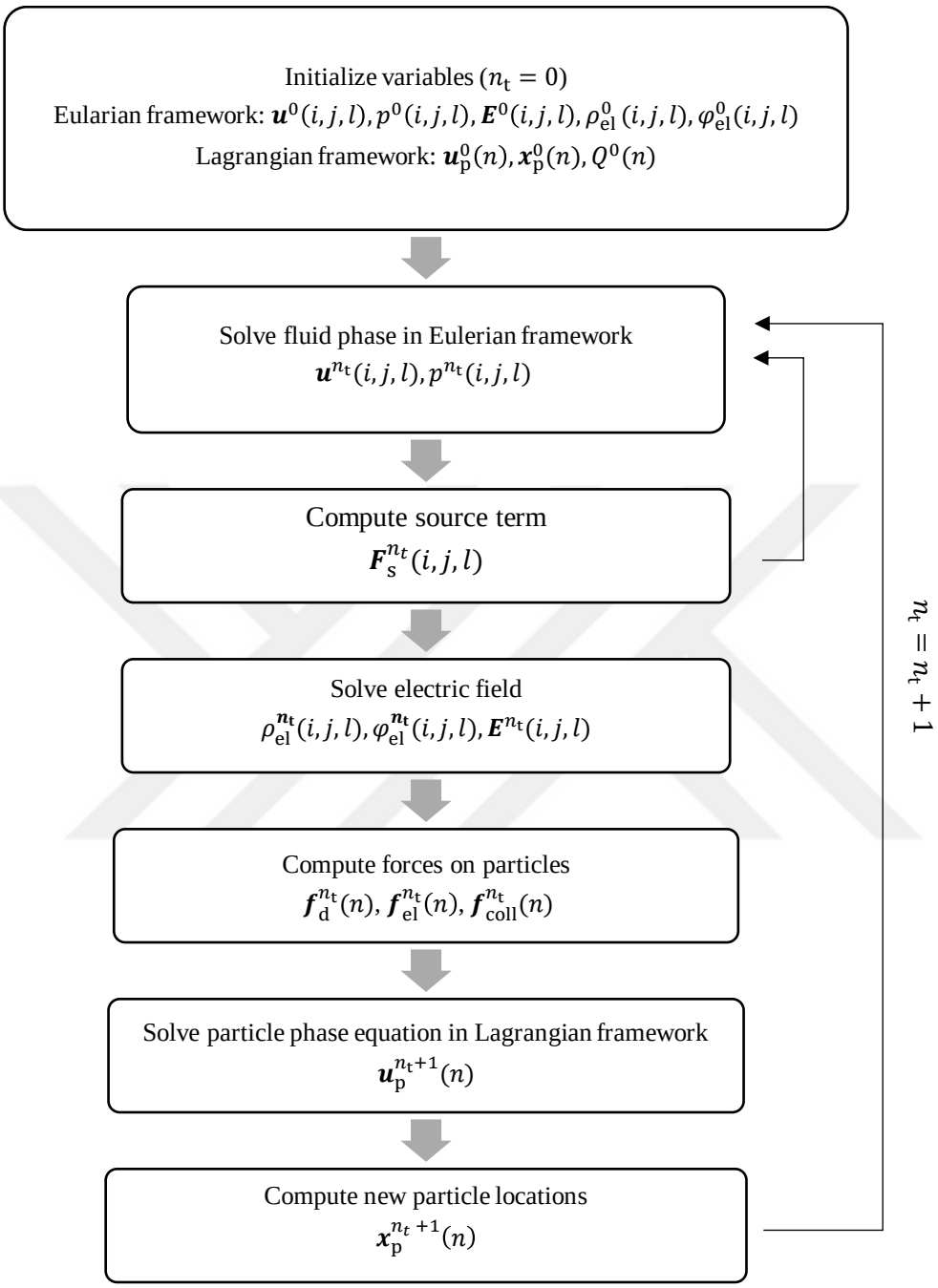
Initialize variables ($n_t = 0$)
Eularian framework: $\boldsymbol{u}^0(i,j,l), p^0(i,j,l), \boldsymbol{E}^0(i,j,l), \rho_{el}^0(i,j,l), \varphi_{el}^0(i,j,l)$
Lagrangian framework: $\boldsymbol{u}_p^0(n), \boldsymbol{x}_p^0(n), Q^0(n)$
Solve fluid phase in Eulerian framework
$\boldsymbol{u}^{n_t}(i,j,l), p^{n_t}(i,j,l)$
Compute source term
$\boldsymbol{F}_s^{n_t}(i,j,l)$
Solve electric field
$\rho_{el}^{\boldsymbol{n_t}}(i,j,l), \varphi_{el}^{\boldsymbol{n_t}}(i,j,l), \boldsymbol{E}^{n_t}(i,j,l)$
Compute forces on particles
$\boldsymbol{f}_d^{n_t}(n), \boldsymbol{f}_{el}^{n_t}(n), \boldsymbol{f}_{coll}^{n_t}(n)$
Solve particle phase equation in Lagrangian framework
$\boldsymbol{u}_p^{n_t+1}(n)$
Compute new particle locations
$\boldsymbol{x}_p^{n_t+1}(n)$
$n_t = n_t + 1$